

# Cardiomyocyte proliferation contributes to heart growth in young humans

Mariya Mollova<sup>a,b,1,2</sup>, Kevin Bersell<sup>a,c,d,1</sup>, Stuart Walsh<sup>a,b</sup>, Jainy Savla<sup>a,c,3</sup>, Lala Tanmoy Das<sup>a,4</sup>, Shin-Young Park<sup>b,e</sup>, Leslie E. Silberstein<sup>e,f</sup>, Cristobal G. dos Remedios<sup>g</sup>, Dionne Graham<sup>a,b</sup>, Steven Colan<sup>a,b</sup>, and Bernhard Kühn<sup>a,b,h,i,5</sup>

Departments of <sup>a</sup>Cardiology and <sup>e</sup>Laboratory Medicine, Boston Children's Hospital, Boston, MA 02115; Departments of <sup>b</sup>Pediatrics and <sup>f</sup>Pathology, Harvard Medical School, Boston, MA 02115; <sup>c</sup>Boston University School of Medicine, Boston, MA 02118; <sup>d</sup>Department of Pharmacology, Vanderbilt University School of Medicine, Nashville, TN 37232; <sup>g</sup>Department of Anatomy, Bosch Institute, The University of Sydney, Sydney, NSW 2006, Australia; <sup>h</sup>Harvard Stem Cell Institute, Cambridge, MA 02138; and <sup>i</sup>Department of Stem Cell and Regenerative Biology, Harvard University, Cambridge, MA 02138

Edited\* by J. G. Seidman, Harvard Medical School, Boston, MA, and approved December 12, 2012 (received for review August 23, 2012)

**The human heart is believed to grow by enlargement but not proliferation of cardiomyocytes (heart muscle cells) during postnatal development. However, recent studies have shown that cardiomyocyte proliferation is a mechanism of cardiac growth and regeneration in animals. Combined with evidence for cardiomyocyte turnover in adult humans, this suggests that cardiomyocyte proliferation may play an unrecognized role during the period of developmental heart growth between birth and adolescence. We tested this hypothesis by examining the cellular growth mechanisms of the left ventricle on a set of healthy hearts from humans aged 0–59 y ( $n = 36$ ). The percentages of cardiomyocytes in mitosis and cytokinesis were highest in infants, decreasing to low levels by 20 y. Although cardiomyocyte mitosis was detectable throughout life, cardiomyocyte cytokinesis was not evident after 20 y. Between the first year and 20 y of life, the number of cardiomyocytes in the left ventricle increased 3.4-fold, which was consistent with our predictions based on measured cardiomyocyte cell cycle activity. Our findings show that cardiomyocyte proliferation contributes to developmental heart growth in young humans. This suggests that children and adolescents may be able to regenerate myocardium, that abnormal cardiomyocyte proliferation may be involved in myocardial diseases that affect this population, and that these diseases might be treatable through stimulation of cardiomyocyte proliferation.**

heart failure | pediatrics

Heart failure, a leading public health problem worldwide (1), is linked to the loss of cardiomyocytes (2–4). The only currently available, definitive therapy—heart transplantation—is limited by donor availability. New approaches, such as cell transplantation, have shown encouraging results in clinical trials (5, 6). However, a third, complementary strategy has emerged, based on stimulating endogenous regenerative mechanisms. One approach for developing such regeneration strategies is to examine the cellular mechanisms of myocardial growth, since mechanisms of regeneration should be similar to the mechanisms of development.

Although stem and progenitor cells are important for morphogenesis of the myocardium, developmental growth in a number of nonhuman species is largely driven by cardiomyocyte proliferation (7–9). In biological models that, unlike adult humans, regenerate myocardium, cardiomyocyte proliferation is important for regeneration as well as postnatal heart growth (10, 11). For example, in mice, developmental cardiomyocyte proliferation continues for up to day 7 after birth, which coincides with the loss of regenerative capacity (11, 12). The close temporal relationship between cardiomyocyte proliferation and heart regeneration in animals raises the question of whether and to what age and extent cardiomyocyte proliferation plays a role in humans. The answer may help us understand the endogenous regenerative potential of the human heart and possibly indicate strategies for stimulating cardiomyocyte proliferation to regenerate myocardium.

Our current understanding of human myocardial growth is limited by an overall lack of reliable data about the underlying cellular mechanisms (reviewed in refs. 3, 4). Cardiomyocyte nuclei have been quantified in human fetuses using hematoxylin-eosin staining (13–15). Radiocarbon birth dating has shown that a small portion of cardiomyocytes is replaced in humans older than 20 y (16), but this technique is unreliable for the analysis of recent samples from individuals younger than 20 y of age (17). The detection of thymidine analogs, used to quantify cardiomyocyte turnover in adult cancer patients (18), is also not feasible in children. Thus, due to multiple limitations, little is known about the cellular growth mechanisms in the human heart in the most dynamic time window between birth and 20 y of age.

Technical limitations have hampered progress in addressing these questions. To overcome these limitations, we have developed and implemented image-based assays. In the present study, we examined a set of 21 healthy young (age range from 0–20 y) hearts and an additional set of 15 adult hearts (*SI Appendix, Table S1*). Our aim was to determine the extent and timing of cardiomyocyte cell cycling, proliferation, and hypertrophy and to relate the activity of these mechanisms to the growth of the human heart.

## Results

**Validation of Sampling and Methods.** Using digital color thresholding on acid Fuchsin Orange G-stained myocardial samples, we quantified fibrosis, which was  $1.02 \pm 0.4\%$ , (Fig. 1A). In addition, we performed histopathologic evaluation of these slides, which led to the elimination of four hearts. Thus, evaluation of the selected hearts showed that they are a representative sample (*SI Appendix, Table S1 and Figs. S1 and S2*).

To be able to use flash-frozen human myocardial samples, we developed a unique isolation method, which involves fixing the myocardium before digestion with collagenase. The resulting yield of cardiomyocytes was  $91.3 \pm 3\%$  [weight%, determined by (original weight – residual)/original weight]. The percentage of cardiomyocytes with desmosome-containing ends was  $92.4 \pm$

Author contributions: M.M., K.B., S.W., C.G.d.R., and B.K. designed research; M.M., K.B., S.W., J.S., L.T.D., and S.-Y.P. performed research; M.M., K.B., S.-Y.P., L.E.S., C.G.d.R., D.G., and S.C. contributed new reagents/analytic tools; M.M., K.B., S.W., J.S., D.G., S.C., and B.K. analyzed data; and M.M., K.B., and B.K. wrote the paper.

The authors declare no conflict of interest.

\*This Direct Submission article had a prearranged editor.

<sup>1</sup>M.M. and K.B. contributed equally to this work.

<sup>2</sup>Present address: Department of Cardiology, University of Heidelberg, 69120 Heidelberg, Germany.

<sup>3</sup>Present address: Department of Medicine, University of California at San Diego, La Jolla, CA 92093.

<sup>4</sup>Present address: Greenberg Division of Cardiology, Weill Cornell Medical College, New York, NY 10021.

<sup>5</sup>To whom correspondence should be addressed. E-mail: bkuehn@enders.tch.harvard.edu.

This article contains supporting information online at [www.pnas.org/lookup/suppl/doi:10.1073/pnas.1214608110/-DCSupplemental](http://www.pnas.org/lookup/suppl/doi:10.1073/pnas.1214608110/-DCSupplemental).

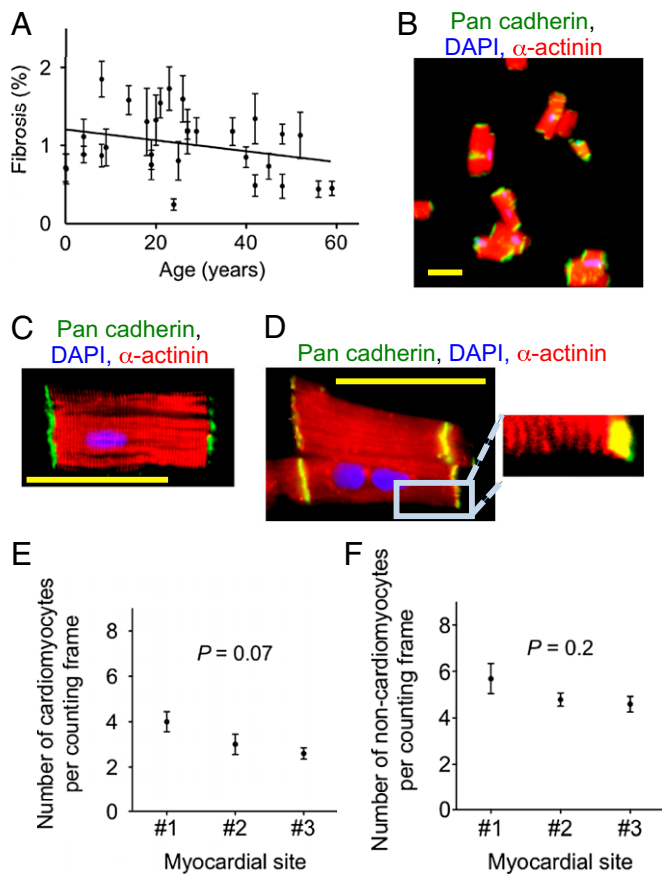


**Fig. 1.** Sampling and isolation methods yield representative probes of healthy human hearts. (A) Analysis of AFOG-stained tissue sections reveals no increased fibrosis; data fitted with linear regression, slope:  $-0.007 \pm 0.002$ ,  $P = 0.007$ . (B) Isolation from a 9-y-old donor heart using the fixation-digestion method yields intact cardiomyocytes. (C) Staining of desmosomes with an antibody against pan-cadherin shows intact cardiomyocytes. (D)  $\alpha$ -actinin shows intact sarcomeres. (E) Optical dissector method quantifying cardiomyocyte and (F) noncardiomyocyte nuclei on three random myocardial sections from different sites of the same LV shows no significant differences in the nuclear density in different compartments of the same LV. Statistical significance was tested with ANOVA. The results are mean  $\pm$  SD. Scale bar: 50  $\mu$ m (B–D).

0.4% (Fig. 1 B and C), and sarcomeres were present (Fig. 1D), indicating that most of the isolated heart muscle cells were intact.

To determine whether immunofluorescence microscopy could reliably differentiate between cardiomyocytes and noncardiomyocytes, we used two different structural markers: a sarcomeric marker ( $\alpha$ -actinin and/or troponin I) as well as a membrane marker (caveolin-3). Confocal microscopy and visual quantification showed agreement between these markers in the identification of cardiomyocyte nuclei (SI Appendix, Fig. S3). We noted that H&E staining overestimated the number of cardiomyocyte nuclei compared with caveolin-3 and troponin I staining (SI Appendix, Fig. S3 G and H). The optical dissector method for quantifying cardiomyocyte (Fig. 1E) and noncardiomyocyte nuclei (Fig. 1F) on three random myocardial sections from different sites of the same left ventricle (LV) showed no significant differences in the nuclear density in different compartments of the same LV, indicating that our sampling method yielded a probe representative of the whole LV. We determined fixation-related tissue shrinkage to be  $21 \pm 5.8\%$  and corrected the results accordingly (SI Appendix, Fig. S6). In summary, the applied sampling methods yield representative probes of human hearts.

### Human Hearts Show Evidence of Cardiomyocyte Cell Cycle Activity.

Having established the validity of our methods, we visualized mitotic cardiomyocytes with antibodies against phosphorylated histone H3 (a marker for M-phase) and sarcomeric markers ( $\alpha$ -actinin, Fig. 2 A and B). Using laser-scanning cytometry (LSC) as an automated and unbiased method for quantification on isolated cardiomyocytes, we determined that during the first year of life the percentage of cardiomyocytes in M-phase was  $0.04 \pm 0.01\%$  ( $n = 6$ , Fig. 2C). Between 10 and 20 y, this decreased to  $0.009 \pm 0.006\%$  ( $n = 5$ ,  $P < 0.05$ , Fig. 2C) and remained detectable in hearts from subjects older than 40 y.

To cross-check these results, we quantified cardiomyocytes in M-phase with a different approach, using confocal microscopy of tissue sections (Fig. 2B, SI Appendix, and Movies S1 and S2). The quantification showed that in the first year of life, the percentage of M-phase cardiomyocytes was  $0.012 \pm 0.003\%$  (Fig. 2D). The percentage of M-phase cardiomyocytes decreased significantly over the first two decades of life but was still detectable above 40 y. The percentages of M-phase cardiomyocytes determined on stained sections correlated well with the results from the LSC analysis of isolated cardiomyocytes, indicating that cardiomyocyte cell cycle activity is higher in young than in adult humans.

Analysis of isolated cardiomyocytes showed that M-phase cardiomyocytes were predominantly mononucleated ( $P < 0.001$ ), which is in agreement with previous reports of cycling mononucleated cardiomyocytes in growing cats (19), rats (20), and mice (21).

### Young Humans Show Evidence of Cardiomyocyte Division.

Detection of the contractile ring provides evidence of cardiomyocyte cytokinesis. The contractile ring consists of regulatory and motor proteins (22), including the mitotic kinesin-like protein (MKLP-1), a component of the centralspindlin complex, which is required for completion of cytokinesis (23). We developed a cardiomyocyte cytokinesis assay by staining thick (30  $\mu$ m) myocardial sections with antibodies against MKLP-1 and  $\alpha$ -actinin (Fig. 3A). Confocal stacks and 3D reconstructions showed contractile rings traversing cardiomyocytes (Movies S3, S4, S5, and S6). For quantification, we identified MKLP-1–positive cardiomyocytes on myocardial sections by confocal microscopy. In the age range of 0–1 y,  $0.016 \pm 0.003\%$  of cardiomyocytes were in cytokinesis ( $n = 6$ ). Between 2 and 10 y, it was  $0.01 \pm 0.002\%$  ( $n = 4$ ), and in the second decade of life, this value decreased to  $0.005 \pm 0.005\%$  ( $n = 5$ ,  $P < 0.05$ , Fig. 3B). We did not detect cardiomyocytes in cytokinesis in subjects older than 20 y ( $n = 9$ ). In summary, human infants show evidence of cardiomyocyte cytokinesis, which decreases during childhood and adolescence to nondetectable levels in adults.

### Human Cardiomyocytes Show an Increase of Nuclear Ploidy with Age.

Cell cycle activity in cardiomyocytes may lead not only to division but also to formation of binucleated and polyploid daughter cells (3). Therefore, to determine the association between cardiomyocyte cell cycle activity and cellular proliferation, it is necessary to account for these nonproductive cell cycles. To determine the percentage of mononucleated cardiomyocytes in our samples, we quantified the number of nuclei in isolated human cardiomyocytes by visual count as well as automatically using LSC (SI Appendix, Fig. S4). The results obtained with both methods were highly correlated (Fig. 4A), thus validating the LSC method. Using LSC, we determined that the percentage of mononucleated cardiomyocytes did not change significantly between the first year ( $67.8 \pm 3\%$ ) and 10 and 20 y of life ( $63.5 \pm 2.2\%$ ,  $P > 0.05$ , Fig. 4B) and remained unchanged throughout life. The percentage of mononucleated cardiomyocytes in children has not been published previously, but the percentage in adults is in agreement with a prior study (24). In conclusion, humans do not display the transition to predominantly binucleated cardiomyocytes,

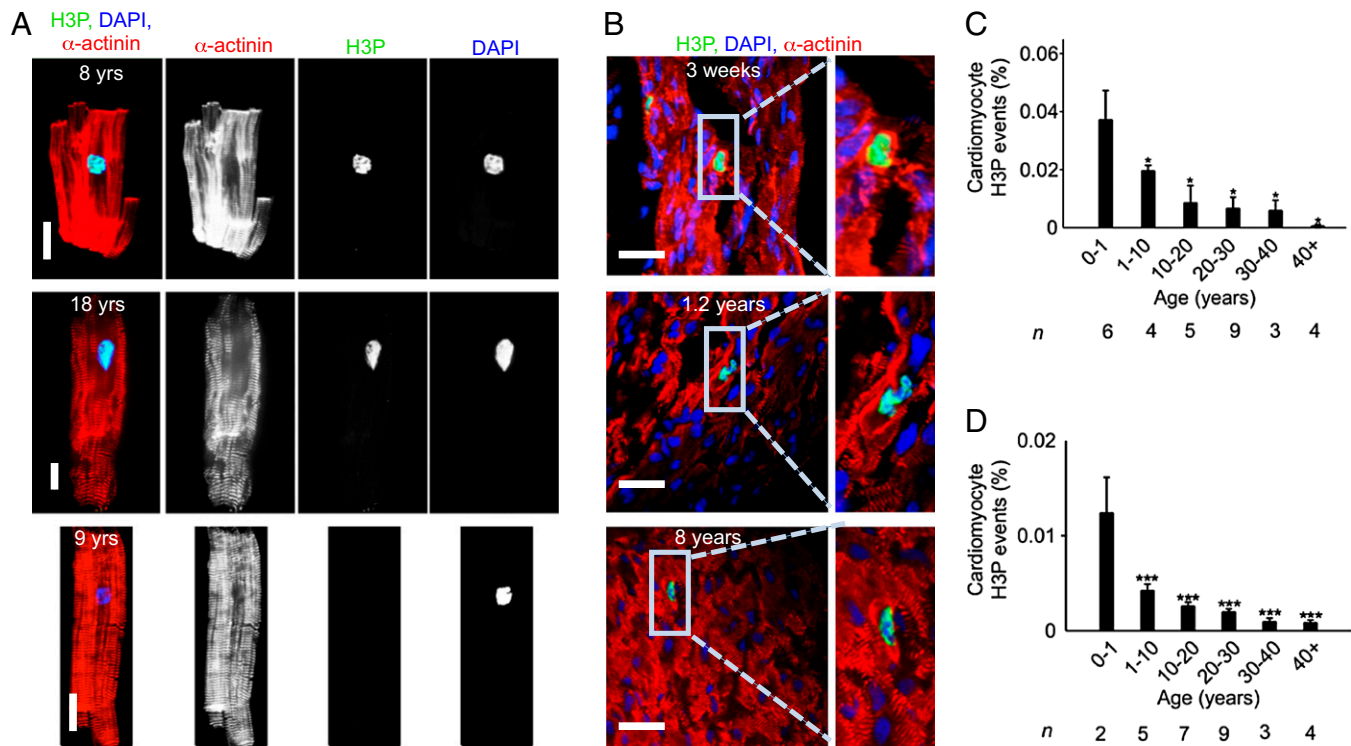


**Fig. 2.** Human hearts show evidence for cardiomyocyte cycling after birth. (A) Isolated cardiomyocytes in M-phase were visualized by immunofluorescent microscopy using antibodies against phosphorylated histone H3 (H3P, green) and  $\alpha$ -actinin (red). H3P-negative cardiomyocyte is shown as a control (Lower). (B) H3P-positive cardiomyocytes on tissue sections. (C and D) Quantification of isolated cardiomyocytes by LSC (C) and on tissue sections (D) shows that the percentage of cycling cardiomyocytes decreases with age. Columns represent mean values of the number of hearts investigated per age group (n) that are indicated under each column. One-way ANOVA revealed a significant difference between 0–1 y and the other age groups. \* $P < 0.05$ , \*\*\* $P < 0.001$ . Scale bar: 25  $\mu$ m.

which is known to happen in murine models in the first week after birth (12, 25).

We examined ploidy changes with LSC and validated them by fluorescence in situ hybridization (FISH) using probes against chromosomes 8 and X (Fig. 4 C and D and *SI Appendix*, Fig. S4). In the first year of life,  $16.3 \pm 5.2\%$  of mononucleated cardiomyocytes were hyperdiploid ( $>2N$ ), which increased to  $39.5 \pm 6.9\%$  between 10 and 20 y ( $P < 0.05$ ), but then remained unchanged (Fig. 4E). Mononucleated polyploid cardiomyocytes increased to  $54.2 \pm 5.8\%$  above 40 y, which was not significantly different compared with 30–40 y. Taking mono- and binucleated cardiomyocytes together, the percentage of those with a total DNA content  $>2N$  increased significantly to  $57.5 \pm 4.5\%$  by 10–20 y, which remained unchanged in later life ( $P < 0.05$ , Fig. 4F). In summary, these results indicate that human cardiomyocytes undergo significant changes in their nuclear ploidy after birth. Together with the result that cycling cardiomyocytes are predominantly mononucleated, this suggests that they are the direct

or indirect precursors of cardiomyocytes with a total DNA content of  $>2N$ .

**Human Cardiomyocytes Proliferate and Enlarge After Birth.** We used stereology techniques to quantify the number of cardiomyocytes per LV (*SI Appendix*). Using the optical dissector principle, we determined that in the first year of life, the volume density of cardiomyocyte nuclei was  $2.4 \pm 0.2 \times 10^8 / \text{cm}^3$  (Fig. 5A). Between 10 and 20 y, the volume density decreased to  $3.6 \pm 0.7 \times 10^7 / \text{cm}^3$  ( $P < 0.05$ ), in agreement with a previous report from adult hearts (26). Using the specific reference volume for each LV (27), we calculated from the volume density of cardiomyocyte nuclei (Fig. 5A) that newborns had  $1.5 \pm 0.9 \times 10^9$  and young adults had  $5.6 \pm 1.5 \times 10^9$  cardiomyocyte nuclei in the LV ( $P < 0.05$ , Fig. 5B). By correcting the number of cardiomyocyte nuclei by accounting for the corresponding percentages of mono- and binucleated cardiomyocytes (from Fig. 4B), we calculated that in the age range of 0–1 y,  $1.1 \pm 0.1 \times 10^9$  cardiomyocytes were present in the LV ( $n = 4$ ), compared with

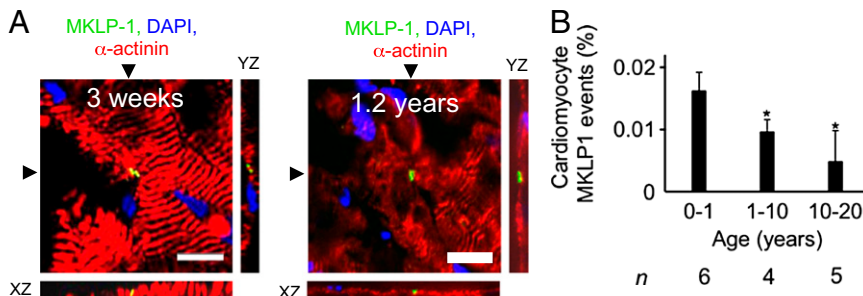


**Fig. 3.** Humans show evidence for cardiomyocyte cytokinesis in the first two decades of life. (A) Cardiomyocyte cytokinesis was detected with an antibody against MKLP-1; XY and XZ reconstruction planes are indicated with arrowheads. (B) Frequency of MKLP-1-positive cardiomyocyte-specific events declines over first two decades of life. Scale bar: 25  $\mu$ m. \* $P < 0.05$  compared with 0–1 y (ANOVA); n, number of hearts analyzed. Cardiomyocyte-specific MKLP-1 activity was not found in samples  $>20$  y of age ( $n = 9$ ). For 3D reconstructions of the photomicrographs in A, see *Movies S3, S4, S5, and S6*.

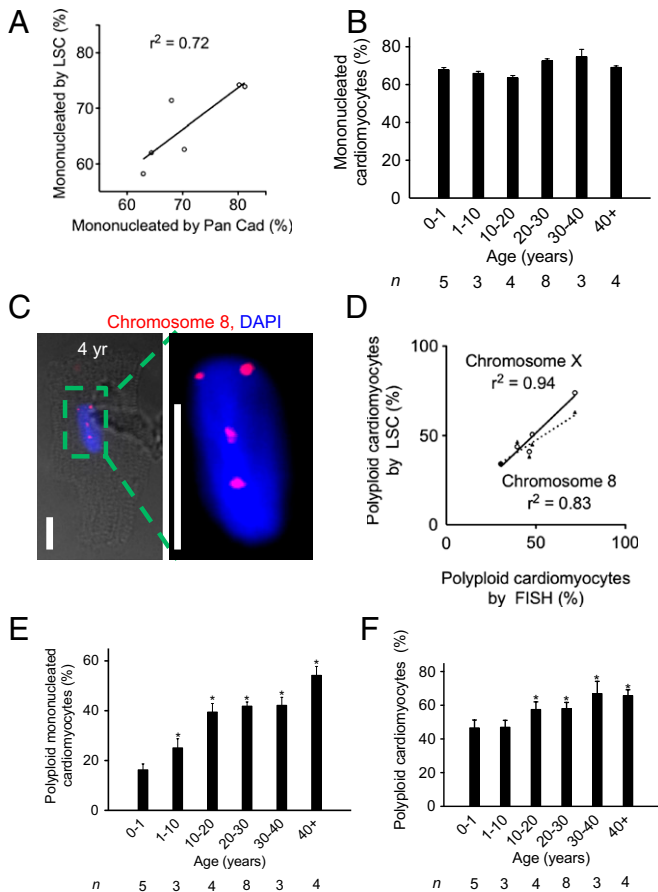


**Fig. 4.** Human cardiomyocytes show increased formation of polyloid nuclei between birth and 20 y. (A) Validation of LSC method for quantification of mononucleated cardiomyocytes. (B) In humans, the percentage of mononucleated cardiomyocytes remains unchanged after birth. (C) Tetraploid cardiomyocyte nucleus (DAPI, blue) with FISH probe against chromosome 8. Scale bar: 25  $\mu$ m. (D) Comparison of quantification of nuclear DNA content using FISH and LSC shows significant correlation. (E) The percentage of polyloid mononucleated cardiomyocytes increases with age. (F) Percentage of cardiomyocytes with DNA content >2N determined by LSC increases with age. Statistical difference between 0–1 y and other age groups was tested with one-way ANOVA: \* $P < 0.05$ .  $n$ , number of hearts analyzed.

$3.7 \pm 0.3 \times 10^9$  at the age of 20 y ( $n = 7$ , Fig. 5C). This represents a 3.4-fold increase ( $P < 0.05$ , Fig. 5C). The mean cellular volume of cardiomyocytes in the age range of 0–1 y was  $5,854 \pm 818 \mu\text{m}^3$  ( $n = 4$ ), and between 10–20 y, it reached  $50,564 \pm 7,398 \mu\text{m}^3$  ( $n = 7$ , Fig. 5D), representing an 8.6-fold increase ( $P < 0.05$ ). Taken together, these results indicate that both cardiomyocyte proliferation and enlargement contribute to postnatal heart growth in humans.

We graphed the number of cardiomyocytes determined in individual LVs (Fig. 5E) and the mean cardiomyocyte volume (Fig. 5F) and fitted the data with LOWESS, validating the fits using generalized cross-validation. The patterns of cardiomyocyte enlargement and proliferation indicated that both contribute simultaneously to myocardial growth between birth and 20 y of age.

**Discussion**

It has long been thought that the number of cardiomyocytes does not change significantly during physiologic postnatal growth in humans (reviewed in ref 3). This notion arose after a 1950 study of human hearts, some of which were diseased. Cardiomyocyte silhouettes were measured on perpendicular sections of the papillary muscles (28), and the results led researchers to conclude

that cardiomyocyte enlargement is the sole mechanism for postnatal growth. By today’s standards, this study was limited by selection, anisotropy, and counting biases (28, 29). Although other reports suggested that cardiomyocytes in human infants show mitotic activity (30–32) and that the number of cardiomyocytes may double in the first year of life (33), the cell-static view has dominated most of our thinking about physiologic heart growth in humans.

Our study demonstrates that myocardial growth in humans is based on two cellular mechanisms: cardiomyocyte enlargement and proliferation. Two lines of evidence support the conclusion that cardiomyocyte proliferation contributes to postnatal myocardial growth. First, we show evidence for cardiomyocyte cytokinesis. Second, we demonstrate that the number of cardiomyocytes increases between birth and 20 y of age. We formally tested the hypothesis that cardiomyocyte cell cycle activity contributes to postnatal cardiomyocyte proliferation by comparing the number of cardiomyocytes predicted to be generated by cell cycle events with the number present in the LV. Calculating the number of cardiomyocytes generated based on cell cycle activity requires input of the incidence of a cell cycle marker (1), the duration of its presence (2), and the probability that the marker indicates division (3). We used the percentage of cardiomyocytes in M-phase, which shows conservation of regulatory mechanisms and duration (~1.5 h) between species, tissues, and ages (34–36). To calculate the number of cardiomyocytes generated from M-phase activity, determined by H3P analysis, we used the previously determined duration of  $1.8 \pm 0.3$  h in adult ventricular cardiomyocytes (21, 37). To correct our results for nonproductive mitotic events (binucleation, polyploidization), we multiplied by the age-specific percentage of mononucleated and diploid cardiomyocytes (from Fig. 4F), which results in the number of actually generated cardiomyocytes. Thus, for the first year of life, the calculation  $0.04\%$  H3P-positive of  $0.9 \times 10^9$  cardiomyocytes (present at birth)  $\times 24 \text{ h} \times 365 \text{ d} / 1.8 \text{ h}$  per mitosis  $\times 56\%$  productive mitoses would yield  $0.9 \times 10^9$  de novo cardiomyocytes in the LV. Using the range of duration of mitosis (1.5–2.1 h) (34) rather than the mean, we calculated a range of  $0.8\text{--}1.1 \times 10^9$  de novo generated cardiomyocyte during the first year of life. In the first decade of life, the same calculation would yield  $\sim 0.9 \times 10^9$  new cardiomyocytes and in the second decade  $0.6 \times 10^9$ . The stereological quantification showed that in the age range of 0–1 y,  $1.1 \pm 0.1 \times 10^9$  ( $n = 4$ ) cardiomyocytes were present and, at 20 y,  $3.7 \pm 0.3 \times 10^9$  ( $n = 7$ ), an increase by  $2.6 \times 10^9$  ( $P < 0.05$ ). Therefore, this cross-check demonstrates that the measured M-phase activity can account for the increase of the number of cardiomyocytes. Considering that a large myocardial infarction can wipe out  $\sim 25\%$  of the adult heart (3), which is equivalent to 1 billion cardiomyocytes, the generation of 2.6 billion new cardiomyocytes during heart growth is significant.

We detected cardiomyocyte proliferation in normal human hearts up to 20 y of age, which is longer than would be anticipated by extrapolating the results from mice (12) and rats (25). In addition, in humans, cardiomyocyte proliferation and enlargement contribute simultaneously to myocardial growth, which contrasts with the rapid switch from proliferation to hypertrophy in mice and rats in the first week of life (12, 25).

Recent studies by Bergmann et al. (16) and Kajstura et al. (38) on generation of cardiomyocytes in human hearts offer an opportunity for comparison with our findings (SI Appendix, Table S5). Using the  $^{14}\text{C}$ -based birth-dating technique, Bergmann et al. (16) reported a turnover rate of 1.9% in one 19 y-old heart and 1% in five hearts between 21–40 y. We calculated that at 20 y  $6.9 \times 10^7$  new cardiomyocytes are generated per year—the equivalent to 1.9% of cardiomyocytes present at this age—based on quantifying cardiomyocyte mitotic activity at 20 y (0.00092% H3P,  $n = 4$ , age range 19–23 y) and adjusting for nonproductive cell cycles. Thus, our results in young adults are within the same range as the corresponding results by Bergmann et al. (16).

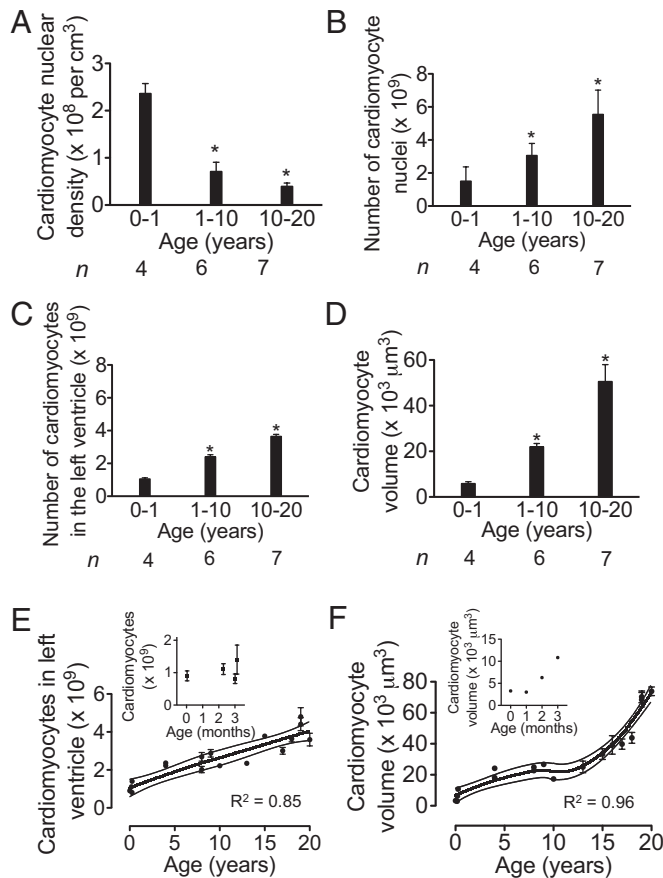


**Fig. 5.** Human cardiomyocytes proliferate and enlarge after birth. (A) Cardiomyocyte nuclear density, determined by the optical disector method, decreases with age. (B) Number of cardiomyocyte nuclei per LV increases with age. (C) Number of cardiomyocytes per LV, calculated from number of cardiomyocyte nuclei (B) and percentages of mono-, bi-, and multinucleated cardiomyocytes. (D) Mean volume of cardiomyocytes increases with age. (E and F) The number (E) and mean volume (F) of cardiomyocytes from individual LVs were graphed over age and modeled using locally weighted scatter plot smoothing (LOWESS). Blow-up graphs of results from the first 3.5 mo of life are shown. Dotted lines indicate 95% confidence intervals.  $R^2$  values are indicated. \* $P < 0.05$ .  $n$ , number of hearts analyzed.

Kajstura et al. (38) reported 0.01% H3P-positive cardiomyocytes between 1–10 y, 0.004% between 10–20 y, 0.003% between 21–40 y, and 0.006% above 40 y. Our corresponding results are 2–3.5-fold higher up to 40 y of age and sixfold lower above 40 y (*SI Appendix*, Table S5). However, Kajstura et al. (38) used their birth-dating results to arrive at cardiomyocyte generation rates that are 5- to 10-fold higher up to 40 y of age and 80-fold higher above 40 y. In contrast, we did not detect cardiomyocyte cytokinesis in hearts from subjects older than 20 y. This may be because, unlike using the mean birthdate of cardiomyocytes, as done by Bergmann et al. (16) and Kajstura et al. (38), our cytokinesis assay is based upon direct visualization and quantification of individual dividing cardiomyocytes. An alternative interpretation of the lack of detection of cardiomyocyte cytokinesis above 20 y is that the corresponding cell cycle activity that we detected using the H3P assay is exclusively associated with nonproductive cell cycle events. In summary, the pattern of cardiomyocyte cell cycle activity in our study, which included more and younger hearts than prior studies, confirms the suggestion that young humans show more cardiomyocyte cycling and division than adults.

The number of generated cardiomyocytes in our stereologic estimates (Fig. 5 C and E) may include those that originate from

cardiogenic stem and progenitor cells, as well as those generated by division of preexisting, differentiated cardiomyocytes. Both mechanisms are not mutually exclusive and may occur simultaneously. Current knowledge of cardiac development would place cardiogenic stem and progenitor cells upstream of dividing cardiomyocytes, but available methods in humans cannot differentiate these two processes (3, 18, 39, 40).

Regardless of the origin of the cycling cardiomyocytes, the findings from our study and others (*SI Appendix*, Table S5) establish the importance of cardiomyocyte proliferation in the growth and development of postnatal human hearts. In addition to providing a new cell-based growth model for the human heart, our findings point to a potential opportunity for stimulating myocardial growth and regeneration in humans—through the manipulation of endogenous mechanisms of cardiomyocyte proliferation.

## Materials and Methods

**Study Population and Tissue Sampling.** The Muscle Research Unit at the University of Sydney (Australia) provided LV myocardial samples from 28 unused donor hearts that were procured for transplantation. The National Institute of Child Health and Human Development Brain and Tissue Bank at the University of Maryland provided eight samples from cadaveric hearts with short post-mortem intervals (*SI Appendix*, Table S1 and Figs. S1 and S2). Sample ascertainment was approved by the Institutional Review Boards of St. Vincent's Hospital (H03/118) and the University of Sydney (09-2009-12146).

**Isolation of Cardiomyocytes from Flash-Frozen Tissue.** Myocardial samples were flash frozen and stored in liquid nitrogen. For isolation, 1 mm<sup>3</sup> blocks of tissue were fixed in 3.7% (vol/vol) normal buffered formaldehyde (Sigma) and incubated on a slow bench top rocker at room temperature for 2 h. The tissue was then washed in PBS for 5 min and digested with collagenase B (1.8 mg/mL, Roche) and collagenase D (2.4 mg/mL, Roche) on a rotator at 37 °C overnight.

**Quantification of Fibrosis.** Myocardial tissue samples were stained with AFOG to visualize cardiomyocytes (red) and collagen (blue), and 15 random images per slide were assessed with a Zeiss Axioplan2 microscope and 20× lens. We quantified the proportion of fibrosis by digital color thresholding (MetaMorph). The same slides were used for histopathologic evaluation.

**Immunofluorescence and Optical Dissector Method.** For each heart, 210 consecutive cryosections were prepared on 70 slides. We selected the initial slide with a random number generator and picked every fifteenth slide after that for staining and microscopy in a random-systematic fashion. Six researchers, blinded with respect to the samples' corresponding ages and identities, quantified cellular events, either by manual count or by digital thresholding (image segmentation and creation of a binary image from a gray scale). Software analysis of the converted binary images was performed with Image Processing and Analysis in Java (Image J). To quantify the number of cardiomyocyte nuclei per cubed centimeter, we used the optical dissector method (29) and validated it with two cardiomyocyte-specific structural markers (*SI Appendix*, Fig. S3). To calculate the number of cardiomyocyte nuclei per LV, we multiplied the number of cardiomyocyte nuclei per cubed centimeter with the LV volume (see below and ref. 27). We quantified tissue shrinkage and corrected all results accordingly (*SI Appendix*, Fig. S6).

**Determination of LV Myocardial Mass.** The LV reference mass of each heart for which heart weight was not available as the mean normal value for body surface area was calculated according to normal z-score values described in ref. 41. Our calculations were based on data from 576 healthy humans obtained at Boston Children's Hospital within an institutional review board-approved study. Quantification of the number of cardiomyocytes per LV using the predicted heart weights matched very closely with estimations based on actual heart weights for those seven hearts where this information was available (*SI Appendix*, Fig. S8).

**Cardiomyocyte Volume Determination.** To determine the cellular volumes of isolated cardiomyocytes, we visualized the cytoplasm with CellMask (Invitrogen, 5 μg/mL, 5 min at room temperature). To select cardiomyocytes for volume analysis, we scanned the stained slide with a ×60 water objective and selected one random cardiomyocyte from every fourth field of view. We acquired confocal stacks with a step size of 1.2 μm (Olympus FV 1000; *SI Appendix*, Fig. S5A). We used digital thresholding to determine the area of

each optical section (*SI Appendix, Fig. S5B*), and by knowing the distance of 1.2  $\mu\text{m}$  between them, we calculated the cellular volume using Image J. The mean of 60–100 isolated cardiomyocytes from each heart was calculated. We validated this design-based method using a model-based method that assumed a cylindrical shape of the cardiomyocyte (24, 25). Bland–Altman analysis (*SI Appendix, Fig. S5 C and D*) revealed a significant agreement between the model-based (24, 25) and our design-based method for volume determination.

**Cell Cycle Activity.** Cardiomyocyte karyokinesis was visualized with an antibody against phosphorylated histone H3 (Ser10, Upstate, 1:500), and cytokinesis was visualized with an antibody against the centralspindlin component MKLP-1 (Abcam, 1:100). Primary antibodies were detected with AlexaFluor conjugated secondary antibodies (Invitrogen; *SI Appendix, Table S4*). Nuclei were visualized with 4',6-diamidino-2-phenylindole (DAPI, Invitrogen, 50 nM).

**Ploidy Determination.** Isolated cardiomyocytes were spread on slides and examined by LSC for observer-independent quantitative analyses of nuclear DNA content (*SI Appendix, Fig. S4*). We validated the LSC-based method of quantifying the amount of DNA in cardiomyocyte nuclei using synchronized human umbilical vein endothelial cells. At least 15,000 cardiomyocytes per sample were analyzed. Ploidy data were further confirmed with FISH probes against chromosomes 8 and X (Vysis), which were visually analyzed.

**Statistical Analysis.** The numbers of analyzed samples and cells are listed in *SI Appendix, Table S3*. Numerical results are represented as means  $\pm$  SEM,

unless otherwise indicated. The age bins were 0–1 y (0–365 d), 1–10 y (366 d–11th birthday), and 10–20 y (after 11th to < 21st birthday) and so forth. Linear regression was used to model the relationship between the proportion of fibrosis vs. age and noncardiomyocyte space vs. age. Continuous outcomes by age group were compared with analysis of variance (ANOVA) followed by Bartlett's post hoc testing. The relationships (mean and 95% confidence interval for the mean) between cardiomyocyte volume and the number of cardiomyocytes per LV vs. age were modeled using locally weighted scatterplot smoothing (LOWESS) (42) to account for nonlinearities in the associations. Generalized cross-validation was used to determine the value of the smoothing parameter that minimized mean squared error. Statistical significance was achieved with a two-sided *P* value < 0.05. Statistical analyses were performed with GraphPad Prism, version 5 for Windows (GraphPad Software) and S-Plus, Version 8.0 (TIBCO Software).

**ACKNOWLEDGMENTS.** We thank R. Mitchell (Brigham and Womens Hospital) for histopathologic evaluation; S. Lal, S. Joseph, and R. Faisal Rasouli (University of Sydney); E. Long, S. Arab, and J. Rosen (Children's Hospital Boston) for technical contributions; and B. Polizzotti, S. Suresh, D. Zebrowski, W. Pu, C. Edwards, and L. Jackson-Grusby for critical suggestions. We acknowledge support from the Department of Cardiology and the Translational Investigator Program (Boston Children's Hospital), the Children's Cardiomyopathy and Gene Foundations (B.K.), the Biomedical Research Exchange Program and the Helmut-Drexler Foundation (M.M.), and the American Heart Association (S.W.). Human heart tissue was obtained from the National Institute of Child Health and Human Development Brain and Tissue Bank for Developmental Disorders.

- Roger VL, et al.; American Heart Association Statistics Committee and Stroke Statistics Subcommittee (2012) Heart disease and stroke statistics—2012 update: A report from the American Heart Association. *Circulation* 125(1):e2–e220.
- Linzbach AJ (1960) Heart failure from the point of view of quantitative anatomy. *Am J Cardiol* 5:370–382.
- Lafamme MA, Murry CE (2011) Heart regeneration. *Nature* 473(7347):326–335.
- Vela D, Buja LM (2008) Quest for the cardiovascular holy grail: Mammalian myocardial regeneration. *Cardiovasc Pathol* 17(1):1–5.
- Bolli R, et al. (2011) Cardiac stem cells in patients with ischaemic cardiomyopathy (SCIPIO): Initial results of a randomised phase 1 trial. *Lancet* 378(9806):1847–1857.
- Siu CW, Tse HF (2012) Cardiac regeneration: Messages from CADUCEUS. *Lancet* 379(9819):870–871.
- Sedmera D, Thompson RP (2011) Myocyte proliferation in the developing heart. *Dev Dyn* 240(6):1322–1334.
- Mercola M, Ruiz-Lozano P, Schneider MD (2011) Cardiac muscle regeneration: Lessons from development. *Genes Dev* 25(4):299–309.
- Yi BA, Wernet O, Chien KR (2010) Regenerative medicine: Developmental paradigms in the biology of cardiovascular regeneration. *J Clin Invest* 120(1):20–28.
- Poss KD, Wilson LG, Keating MT (2002) Heart regeneration in zebrafish. *Science* 298(5601):2188–2190.
- Porrello ER, et al. (2011) Transient regenerative potential of the neonatal mouse heart. *Science* 331(6020):1078–1080.
- Soonpaa MH, Kim KK, Pajak L, Franklin M, Field LJ (1996) Cardiomyocyte DNA synthesis and binucleation during murine development. *Am J Physiol* 271(5 Pt 2):H2183–H2189.
- Austin A, Fagan DG, Mayhew TM (1995) A stereological method for estimating the total number of ventricular myocyte nuclei in fetal and postnatal hearts. *J Anat* 187 (Pt 3):641–647.
- Mayhew TM, Pharaoh A, Austin A, Fagan DG (1997) Stereological estimates of nuclear number in human ventricular cardiomyocytes before and after birth obtained using physical disectors. *J Anat* 191(Pt 1):107–115.
- Mayhew TM, Gregson C, Pharaoh A, Fagan DG (1998) Numbers of nuclei in different tissue compartments of fetal ventricular myocardium from 16 to 35 weeks of gestation. *Virchows Arch* 433(2):167–172.
- Bergmann O, et al. (2009) Evidence for cardiomyocyte renewal in humans. *Science* 324(5923):98–102.
- Spalding KL, Buchholz BA, Bergman LE, Druid H, Frisén J (2005) Forensics: Age written in teeth by nuclear tests. *Nature* 437(7057):333–334.
- Kajstura J, et al. (2010) Cardiomyogenesis in the adult human heart. *Circ Res* 107(2):305–315.
- Chen X, et al. (2007) Adolescent feline heart contains a population of small, proliferative ventricular myocytes with immature physiological properties. *Circ Res* 100(4):536–544.
- Kühn B, et al. (2007) Periostin induces proliferation of differentiated cardiomyocytes and promotes cardiac repair. *Nat Med* 13(8):962–969.
- Bersell K, Arab S, Haring B, Kühn B (2009) Neuregulin1/ErbB4 signaling induces cardiomyocyte proliferation and repair of heart injury. *Cell* 138(2):257–270.
- Fededa JP, Gerlich DW (2012) Molecular control of animal cell cytokinesis. *Nat Cell Biol* 14(5):440–447.
- Lewellyn L, Carvalho A, Desai A, Maddox AS, Oegema K (2011) The chromosomal passenger complex and centralspindlin independently contribute to contractile ring assembly. *J Cell Biol* 193(1):155–169.
- Olivetti G, et al. (1996) Aging, cardiac hypertrophy and ischemic cardiomyopathy do not affect the proportion of mononucleated and multinucleated myocytes in the human heart. *J Mol Cell Cardiol* 28(7):1463–1477.
- Li F, Wang X, Capasso JM, Gerdes AM (1996) Rapid transition of cardiac myocytes from hyperplasia to hypertrophy during postnatal development. *J Mol Cell Cardiol* 28(8):1737–1746.
- Tang Y, Nyengaard JR, Andersen JB, Baandrup U, Gundersen HJ (2009) The application of stereological methods for estimating structural parameters in the human heart. *Anat Rec (Hoboken)* 292(10):1630–1647.
- Sluysmans T, Colan SD (2005) Theoretical and empirical derivation of cardiovascular allometric relationships in children. *J Appl Physiol* 99(2):445–457.
- Linzbach AJ (1950) [The muscle fiber constant and the law of growth of the human ventricles]. *Virchows Arch* 318(5):575–618.
- Mühlfeld C, Nyengaard JR, Mayhew TM (2010) A review of state-of-the-art stereology for better quantitative 3D morphology in cardiac research. *Cardiovasc Pathol* 19(2):65–82.
- Macmahon HE (1937) Hyperplasia and regeneration of the myocardium in infants and in children. *Am J Pathol* 13(5):845–854.
- Chang KT, Taylor GP, Meschino WS, Kantor PF, Cutz E (2010) Mitogenic cardiomyopathy: A lethal neonatal familial dilated cardiomyopathy characterized by myocyte hyperplasia and proliferation. *Hum Pathol* 41(7):1002–1008.
- Zerbini C, Weinberg DS, Perez-Atayde AR (1992) DNA ploidy analysis of myocardial hyperplasia. *Hum Pathol* 23(12):1427–1430.
- Adler CP, Costabel U (1975) Cell number in human heart in atrophy, hypertrophy, and under the influence of cytostatics. *Recent Adv Stud Cardiac Struct Metab* 6:343–355.
- Hahn AT, Jones JT, Meyer T (2009) Quantitative analysis of cell cycle phase durations and PC12 differentiation using fluorescent biosensors. *Cell Cycle* 8(7):1044–1052.
- Shi Q, King RW (2005) Chromosome nondisjunction yields tetraploid rather than aneuploid cells in human cell lines. *Nature* 437(7061):1038–1042.
- Carney BK, Caruso Silva V, Cassimeris L (2012) The microtubule cytoskeleton is required for a G2 cell cycle delay in cancer cells lacking stathmin and p53. *Cytoskeleton (Hoboken)* 69(5):278–289.
- Bettencourt-Dias M, Mittnacht S, Brockes JP (2003) Heterogeneous proliferative potential in regenerative adult newt cardiomyocytes. *J Cell Sci* 116(Pt 19):4001–4009.
- Kajstura J, et al. (2012) Cardiomyogenesis in the aging and failing human heart. *Circulation* 126(15):1869–1881.
- Steinhauser ML, Lee RT (2011) Regeneration of the heart. *EMBO Mol Med* 3(12):701–712.
- Ferreira-Martins J, et al. (2012) Cardiomyogenesis in the developing heart is regulated by c-kit-positive cardiac stem cells. *Circ Res* 110(5):701–715.
- Foster BJ, et al. (2008) A novel method of expressing left ventricular mass relative to body size in children. *Circulation* 117(21):2769–2775.
- Cleveland WS, Dvelin SJ (1988) Locally-weighted regression: An approach to regression analysis by local fitting. *J Am Stat Assoc* 83(403):596–610.

## **Supplemental Appendix**

### **Cardiomyocyte proliferation contributes to post-natal heart growth in humans**

Mariya Mollova, Kevin Bersell, Stuart Walsh, Jainy Savla, Lala Tanmoy Das, Shin-Young Park, Leslie Silberstein, Cristobal G. dos Remedios, Dionne Graham, Steven Colan, and Bernhard Kühn

**Supplemental Information** for this manuscript include:

**Supplemental Experimental Procedures**

**Supplemental Figures and Legends S1–S8**

**Supplemental Tables S1–S5**

**Supplemental References**

## **Supplemental Experimental Procedures**

### **Preparation of myocardial samples from healthy human hearts (Sydney, Australia):**

Obtaining high-quality myocardial samples from newborn babies and young children was a major technical challenge that we needed to overcome in order to accomplish the goals of our study. The muscle research institute at the University of Sydney (Australia) has a tissue bank with healthy human hearts that were procured for transplantation and hence subjected to a strict quality control (short post-mortem interval, standardized preservation procedures). All hearts were removed from the donor and back-flushed with ice-cold cardioplegic solution to remove as much blood as possible (histology showed that there were only occasional blood cells left). They were then double-bagged under sterile conditions and transported by jet plane to the tissue bank in Sydney (**Suppl. Fig. S1A**). The left ventricular (LV) wall was cut from base to apex along the line where the anterior free wall meets the interventricular septum (**Suppl. Fig. S1B**). This process was repeated for the posterior LV wall. The subauricular and subatrial papillary muscles were removed and the remaining tissue was cut into approximately 1 cm-wide strips of the LV free wall and then divided into smaller (1 g) pieces that were immediately flash frozen and then stored in liquid nitrogen (**Suppl. Fig. S1C, D**). The samples were sent to Children's Hospital Boston, embedded in random orientation (OCT, Triangle Biomedical Sciences) and stored in a  $-80^{\circ}\text{C}$  freezer. We prepared cryosections (14 and 30  $\mu\text{m}$ ) with a cryostat (CM3050S, Leica) and adhered three consecutive sections per slide to positively charged glass slides (Colorfrost, Fisher).

**Preparation of myocardial samples from human cadaveric hearts (Baltimore, USA):** We selected hearts from the NICHD Brain and Tissue Bank for Developmental Disorders

(University of Maryland, Baltimore, MD). The samples had post-mortem times of less than 24 hr, were flash-frozen, and stored in liquid nitrogen. These myocardial samples were then processed in the same way as the samples from donor hearts (**Suppl. Fig. S2, Suppl. Tab. S1**).

**Analysis on myocardial sections:** We selected slides for staining in a random-systematic fashion[1]; that is we selected the first slide to be between number 1 and 10 with a random number generator and then selected every fifteenth slide. We prepared 210 consecutive sections for every heart, three sections per slide, which we coded in such a way that the age of the sample was not identifiable by the analyzing researchers. To quantify myocardial fibrosis, we stained 15 cryosections per heart with acid fuchsin orange-G (AFOG) and took 15 random images on each section (Zeiss AxioPlan2,  $\times 20$  lens). We quantified scar size from these images using Metamorph software *via* digital color thresholding (Metamorph, Molecular Devices). Cardiomyocytes and their nuclei were identified using two different structural markers (troponin I and caveolin 3, **Suppl. Fig. S3**); 15 random images per slide were taken with Olympus IX-81 epifluorescence microscope,  $\times 60$  lens) and number of nuclei was quantified using the optical dissector method<sup>1</sup>.

Six blinded observers, unaware of the samples' corresponding ages, performed all quantifications.

**Validation of the method for identifying cardiomyocyte nuclei using immunofluorescent microscopy:** Sections from human neonatal and adult hearts were stained with cardiomyocyte-specific antibodies against troponin I and caveolin 3. Nuclei were stained with DAPI. Cardiomyocytes were identified in counting frames ( $131 \times 131 \mu\text{m}$ ) using both structural markers and counted with the optical dissector method. Counts were compared by linear

regression analysis. There was a significant correlation between both methods for cardiomyocyte identification  $r^2=0.8$ . Bland Altman analysis demonstrated substantial agreement between the two methods for cardiomyocyte quantification (**Suppl. Fig. S3**).

**Analysis of isolated cardiomyocytes using laser-scanning cytometry (LSC):** Using an automatized method, such as an LSC platform, enabled us to perform analysis on large populations of heart muscle cells in an unbiased, observer-independent fashion. The isolated cardiomyocytes were blocked in blocking medium (5% goat serum, 0.05% Tween-20 in  $\text{Ca}^{2+}$ -free,  $\text{Mg}^{2+}$ -free D-PBS) for 10 min before immunofluorescent staining with antibodies against phosphorylated histone H3 (Ser10, rabbit, 1:500, Upstate) and sarcomeric  $\alpha$ -actinin (mouse, 1:500, Sigma). The primary antibodies were visualized with anti-mouse Alexa 564 and anti-rabbit Alexa 488 conjugated secondary antibodies (Invitrogen). Nuclei were then labelled with 50 nM DAPI (Invitrogen) and the cardiomyocyte suspensions were spread on glass slides. Coverslips (no. 1.5, VWR) were placed on cardiomyocytes in a water suspension. For LSC analyses, the iCys<sup>®</sup> Research Imaging Cytometer (CompuCyt Corp.) with four excitation lasers (405, 488, 561, and 633 nm), four emission filters (430-470, 500-545, 565-595, 650 nm long pass), and four photomultiplier tubes (PMT), each detecting a specific wavelength range, was used. PMT signals were converted into 14-bit pixel values that were assembled into high-resolution images at an X step size of 1  $\mu\text{m}$  per pixel. The quantitative imaging cytometry control software (CompuCyt Corp.) generated a sequence of high-magnification (20x objective) ‘field’ immunofluorescence images which were subjected to automated analysis of contour-based cellular events, nuclear events, and their fluorescence levels. For each fluorescent marker, images were built pixel by pixel from the quantitative PMT measurements of laser-spot-excited fluorescence[2]. Individual cellular events were defined by threshold contouring of  $\alpha$ -actinin stained cytoplasm. Individual nuclear events were defined by threshold contouring of DAPI

stained nuclei. The numbers of nuclei in each cell were defined by nuclear events within the integration contour of cellular events. The integration contour was set as 7 pixels out from the threshold contour of cellular events (pixel size was 1  $\mu\text{m}$  x 0.491  $\mu\text{m}$ ). The total fluorescence intensity of H3P was measured in the green channel within the integration contour of cellular events. Ploidy quantifications were performed on the basis of DAPI nuclear staining (blue), which allows analysis of both DNA content (integral value) and chromatin concentration (maximum pixel intensity). We validated the LSC-based method of quantifying the amount of DNA in each cardiomyocyte nucleus using human umbilical vein endothelial cells, which are known to be diploid (2N), as control (**Suppl. Fig. S4**). At least 15,000 cardiomyocytes per heart were analyzed per sample.

#### **Validation of ploidy measurement using human umbilical vein endothelial cells as diploid**

**control:** Laser-scanning cytometry (LSC), FACS, measures the relative amount of fluorescence. To calibrate the DNA quantification, obtained with LSC, we used synchronized human umbilical vein endothelial cells (HUVEC, Lonza, cc-251). G1/S phase cell cycle arrest was induced with double thymidine block. HUVEC were cultured in EGM<sup>®</sup>-2 Endothelial Cell Growth Medium-2 (Lonza CC-3156) media to confluence in serum rich-media supplemented with FBS, hydrocortisone, hFGF-B, VEGF, R3-IGF-1, ascorbic acid, hEGF, GA-1000, and heparin (10% FCS, 1% Pen-Strep, 1% glutamine) and 2 mM thymidine (Sigma T1895-1G) for 16 hours. Cells were washed 3 x with PBS and fresh EndoGRO added to release cells for 9 hours. After releasing, cells were cultured in serum-rich media with 2 mM thymidine for an additional 17 hours. Thereafter, cells were washed in PBS, trypsinized and fixed in 3.7% paraformaldehyde. HUVEC cells were washed 3x PBS and spun down 3000 rpm. Cells were stained with Cell Mask<sup>™</sup> (Invitrogen C10045) and DAPI. Cells washed 2 x PBS and dehydrated onto polylysine-charged slides and cover-slipped. Ploidy was assessed by LSC (**Suppl. Fig. S4j**).

**Microscopy and immunofluorescence:** To identify desmosomes, we used a rabbit anti-pan-cadherin (Sigma, Cat# C3678, 1:500) and to identify cardiomyocyte cell membranes we used a mouse caveolin 3 antibody (Cat#610421, BD Transduction Labs, 1:100). To identify cardiomyocyte sarcomeres, we used primary antibodies against tropomyosin (Developmental Studies Hybridoma Bank, 1:100) and sarcomeric  $\alpha$ -actinin (Sigma, 1:500), and coupled them with Alexa-fluorophore-conjugated secondary antibodies (Invitrogen) (**Suppl. Tab. S4**). Nuclei were visualized with 4', 6'-diamidino-phenylindole (DAPI, Invitrogen, 1:5000). The  $\gamma$  value for image acquisition was set at one. Lookup table settings were linear. Karyokinesis was visualized with an antibody against phosphorylated histone H3 (Upstate, 1:500) and a monoclonal antibody against the centralspindlin component MKLP-1 (Abcam, 1:100) was used to detect cytokinesis. Images were obtained using a spinning disk confocal microscope (DSU, Olympus) and a laser-scanning confocal microscope (FV1000, Olympus) (**Suppl. Tab. S2**). Three-dimensional reconstructions of the MKLP-1 positive events are shown as separate movies (**Supplemental Movies S1-S4**).

**Quantification of mean cardiomyocyte volume:** To determine the cellular volumes of isolated cardiomyocytes, we visualized the cytoplasm with CellMask (5  $\mu\text{g}/\text{mL}$ , 5 min incubation at room temperature, Invitrogen) and spread the cardiomyocytes on slides. To select cardiomyocytes for volume analysis, we scanned the stained slide with a  $\times 60$ - water lens and selected one random cardiomyocyte from every 4<sup>th</sup> field of view. We acquired confocal stacks with a step size of 1.2  $\mu\text{m}$  (Olympus FV 1000, **Suppl. Fig. S5a**). We used digital thresholding to determine the area of each optical section (Image J, **Suppl. Fig. S5b**). Using the area of each optical section and the 1.2  $\mu\text{m}$  between them, we computed the cellular volume. The average cardiomyocyte volume for each heart was determined by calculating the mean  $\pm$  SEM of 60-100 isolated cardiomyocytes from each heart.

**Comparison of design-based and model-based stereological methods for quantification of cardiomyocyte cell volume:** In order to validate our cardiomyocyte volume analysis, we applied two different methods. We first used digital color thresholding in 3D- reconstructions of confocal Z-stack images of isolated heart muscle cells and then compared this design-based method to a model that assumed a cylindrical shape for the cardiomyocytes<sup>2</sup>. We performed a Bland-Altman test to determine the agreement between the two methods and a linear regression analysis to see whether the difference between the two methods changed with changing size of the cardiomyocytes. A total of 129 young and 127 adult cardiomyocytes were investigated.

The results show a significant agreement between our designed-based method and model-based methods that have been previously reported in the literature<sup>2</sup>. *P*- values in both the young and the adult hearts were < 0.05, indicating a significant agreement of both methods, irrespective of age (**Suppl. Fig. S5c,d**).

**Quantification of tissue shrinkage:** Fixation and staining procedures inevitably lead to tissue shrinkage- a factor that should be considered when quantifying events on three- dimensional tissue sections in order to avoid introducing systematic bias to the volume analyses.

To determine tissue shrinkage in x and y direction, we measured the area per point on phase images of our sections, overlaid with a grid of known dimensions (grid point method)[3] (**Suppl. Fig. S6**). The area per point *a* (point) is the product of the distances between points in the x- and y –directions. The number of points *P* hitting the profile of a section was counted and the total area of a section *A* was estimated according to the formula:  $A = \sum P \times a(p)$ . Measurements before and after fixation and staining were made and the percentage of tissue area shrinkage was calculated.

For tissue shrinkage estimation in the z-dimension, using confocal microscopy, a Z-stack was taken across the whole depth of a section prior to and after fixation and staining procedures. The

thickness of each section was determined at 10 random spots for every section by using the full width at half maximum (FWHM) intensity after plotting the projection of the corresponding grey value profile in Image J. (**Suppl. Fig. S6**). The combination of xy- and z-dimensional measurements resulted in a correction factor of  $21 \pm 5.8\%$  (mean  $\pm$  SEM) for tissue shrinkage upon fixation and staining.

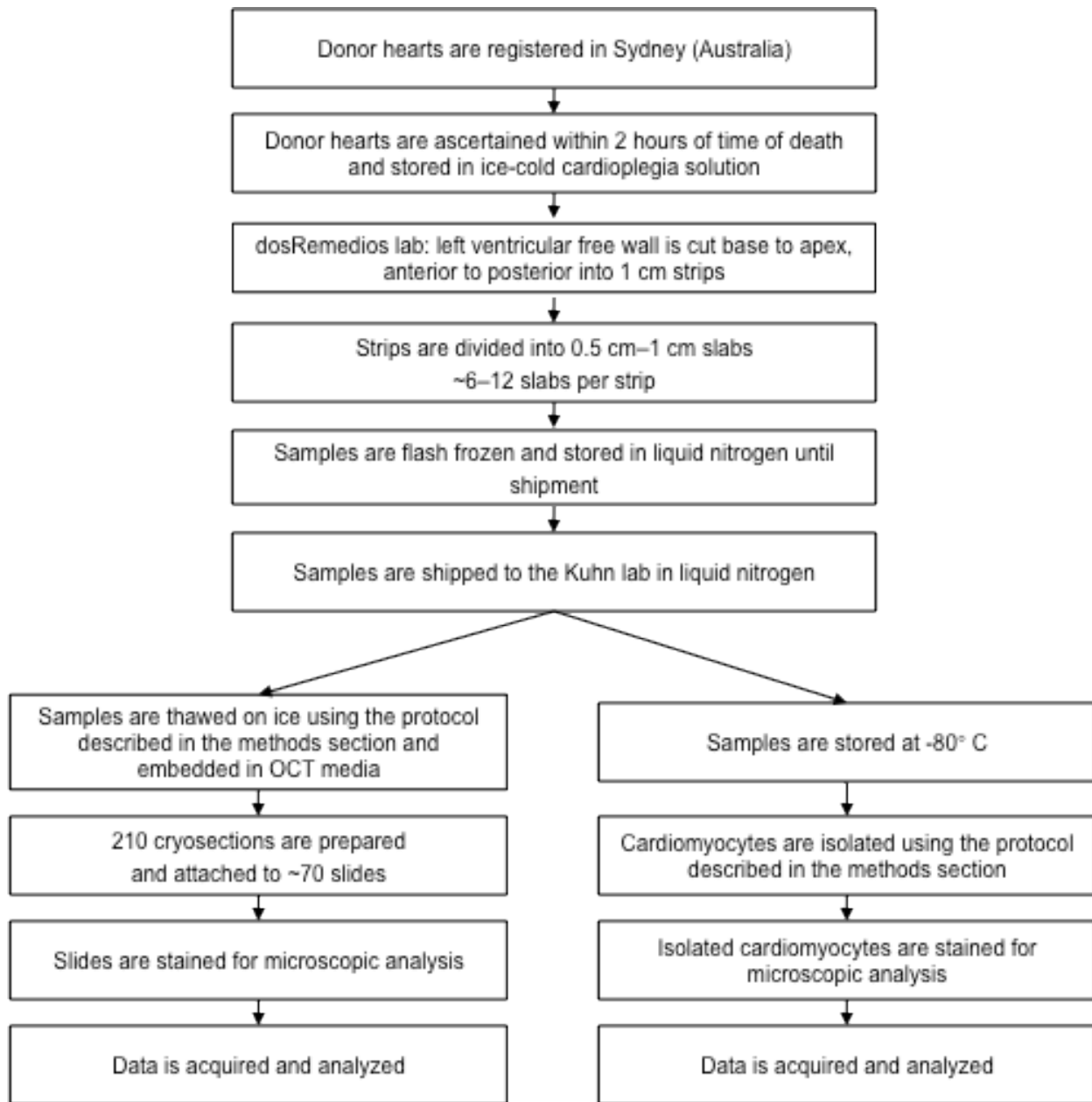
**Quantification of the number of cardiomyocytes per heart:** Cardiomyocyte nuclei were counted using the optical dissector method[1] on 14  $\mu\text{m}$  cryosections that were stained with  $\alpha$ -actinin or tropomyosin to identify cardiomyocytes and with DAPI to identify nuclei. We used a spinning disc confocal microscope (Olympus DSU) with a 60x water lens to capture two confocal slices, which were 5  $\mu\text{m}$  apart in the z-axis. One image was used as the counting plane and the other as lookup plane, as described[1,4]. In the counting plane, we counted only those nuclei that were completely surrounded by cardiomyocyte cytoplasm and that were absent from the lookup plane. For this analysis, the first slide from each sample was selected to be between number 1 and 10 using a random number generator. The next slide was selected by successively adding 10 to the random number. Three random sample volumes were counted in this way per section, amounting to 15 sample volumes per heart. The number of cardiomyocyte nuclei per LV was calculated by multiplying the number of cardiomyocyte nuclei per  $\text{cm}^3$  (cardiomyocyte nuclear density) with the LV reference volume[5].

**Determination of LV reference volume:** Weight is the recommended stereological parameter to determine the reference myocardial volume of the heart[1,4]. Exact donor heart weights were available for 7 of the samples studied. To assess LV myocardial growth[5] for the rest of the samples, echocardiographic data from 576 healthy humans in the age range 0-20 years were

obtained from an IRB-approved study at Children's Hospital Boston. The relationship of BSA to myocardial mass was determined using the LMS method as described in [6]. The LV mass for each donor heart was calculated as the mean predicted left ventricular mass for body surface area based on the relationship determined in this normal population. Quantification of stereological parameters of the heart using the calculated heart weights matched very closely with estimations based on actual heart weights for those hearts where this information was available (**Supplemental Figure S8**).

## Supplemental Figure and Legend S1

a

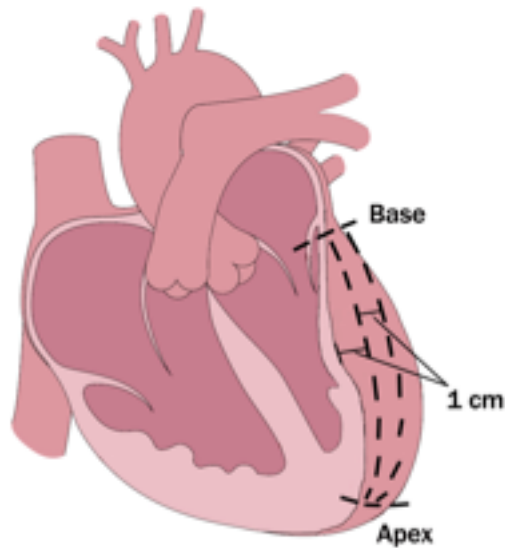


### Supplemental Figure S1. Workflow from donor hearts to sample analysis.

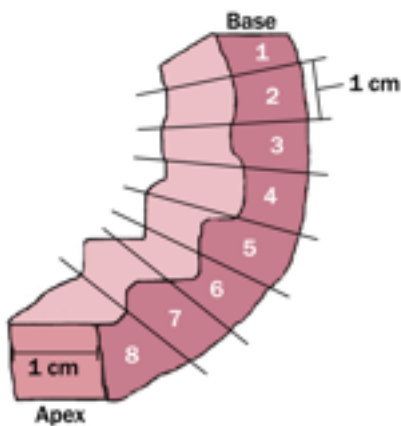
(a) Flow diagram highlights the key steps of tissue collection, sample acquisition, storage, transportation and analysis.

**Supplemental Figure and Legend S1, continued.**

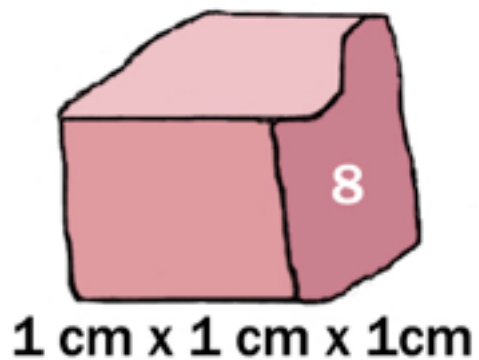
**b**



**c**



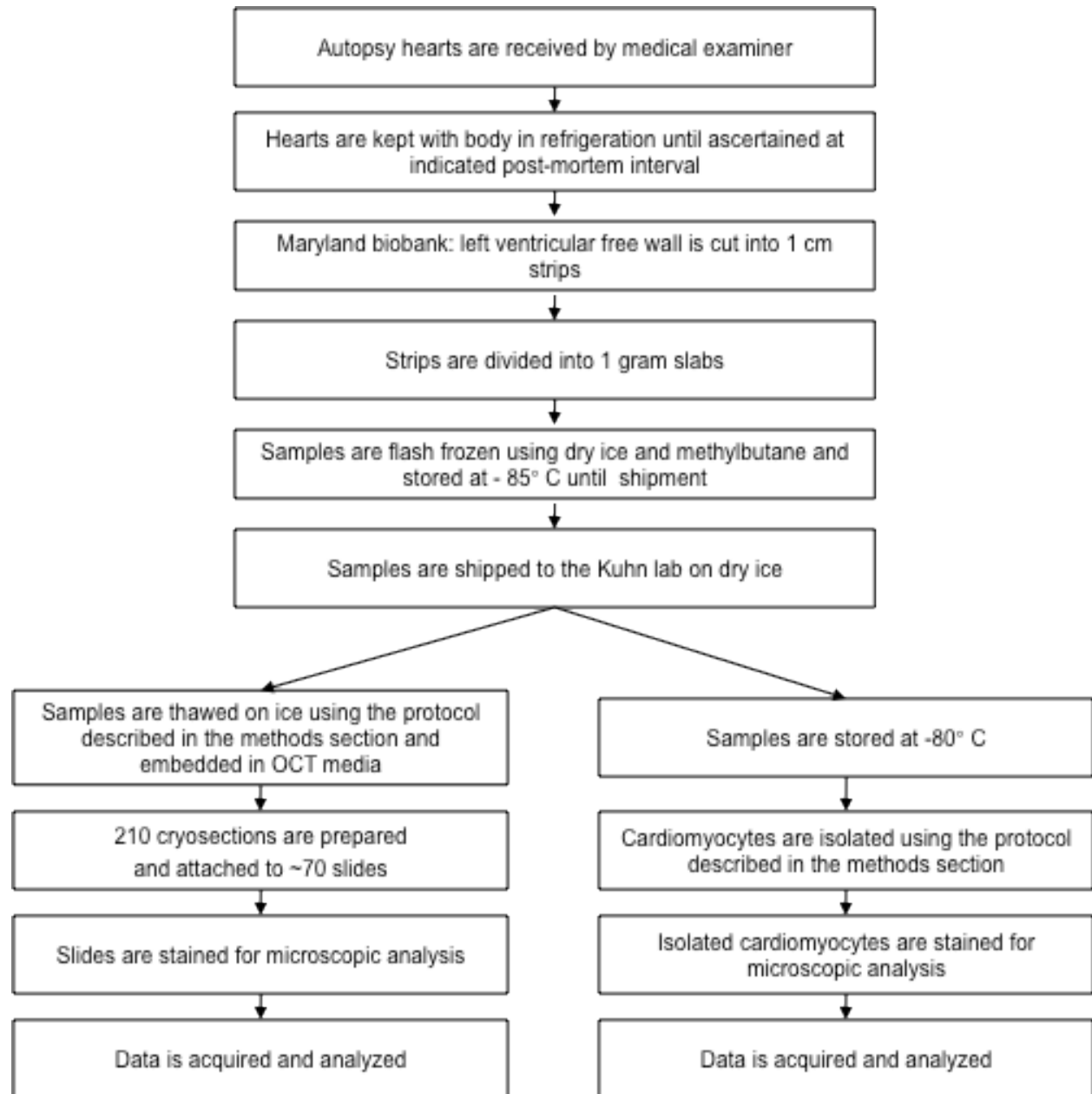
**d**



**Supplemental Figure S1, continued. Workflow from donor hearts to sample analysis.**

(b) After cutting along the anterior margin between the interventricular septum and the left ventricular free wall from the base to the apex, parallel strips of myocardium were cut in 1 cm distance, moving from anterior to posterior. (c) The 1 cm strips were then divided into 1 cm x 1 cm cubes and flash-frozen in liquid nitrogen. The time from removing the heart from cardioplegia solution to freezing of the last sample was less than 45 min. (d) Diagram of one myocardial sample used for analysis.

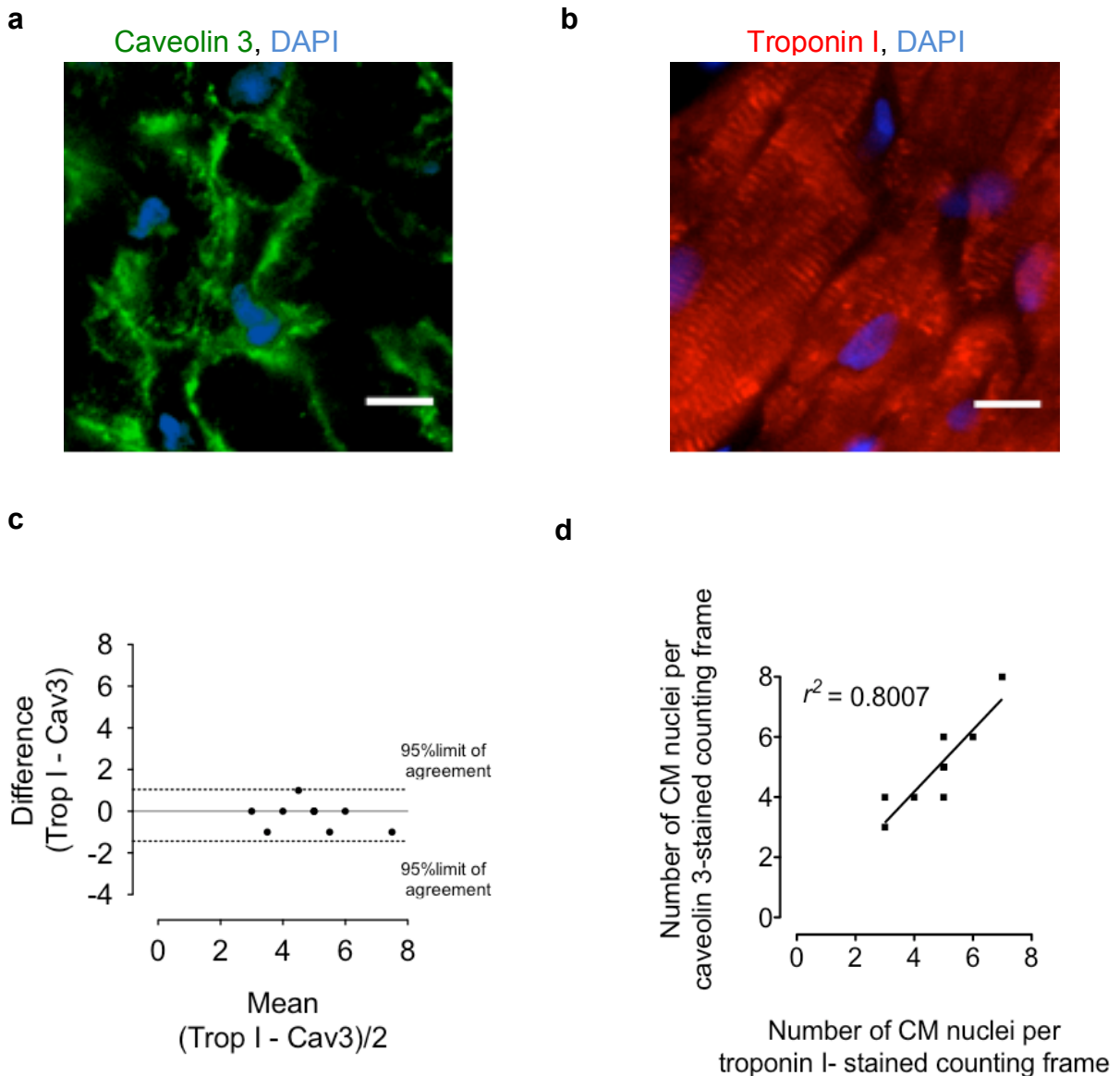
## Supplemental Figure and Legend S2



### Supplemental Figure S2. Workflow from sample ascertainment to data analysis for cadaveric hearts.

The hearts from the Maryland Hybridoma tissue bank were obtained from human cadavers within 4-23 hr of death. The hearts were kept refrigerated with the body until the medical examiner provided the body to the University of Maryland. They were cut into smaller samples, and flash-frozen with dry ice and methylbutane.

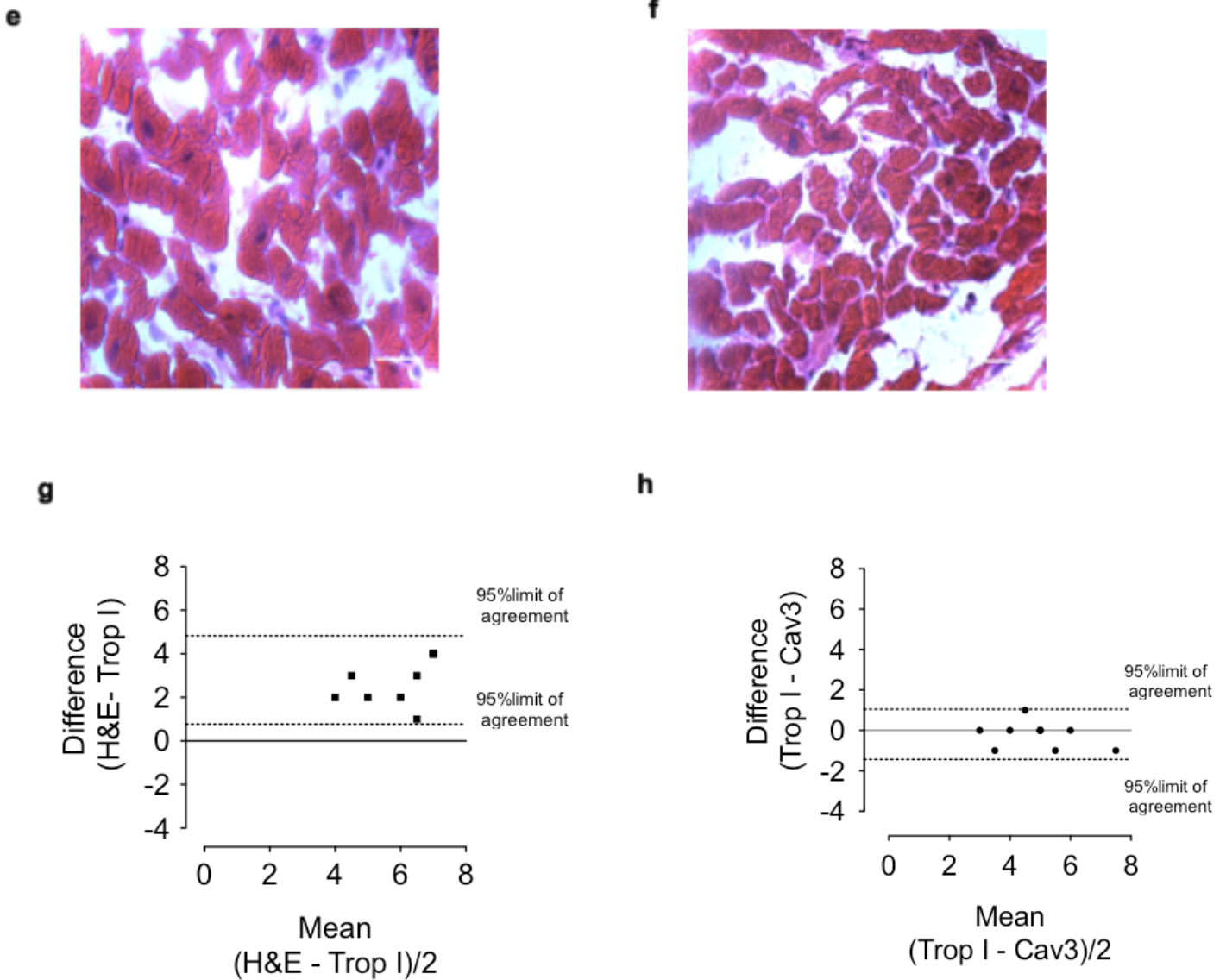
### Supplemental Figure and Legend S3



### Supplemental Figure S3. Validation of the immunofluorescent identification of cardiomyocytes for the optical dissector method.

Sections from human neonatal and adult hearts were stained with antibodies against troponin I and caveolin 3. Nuclei were stained with DAPI. Cardiomyocytes were identified in counting frames (131 x 131 $\mu$ m) and counts were analyzed by linear regression. (a) Caveolin 3 staining. (b) Troponin I staining, Scale bar 10  $\mu$ m. (c) Bland Altman analysis demonstrates agreement between the two methods for cardiomyocyte quantification. (d) Linear regression demonstrates a high correlation between the number of cardiomyocytes identified by caveolin 3 and troponin I antibody.

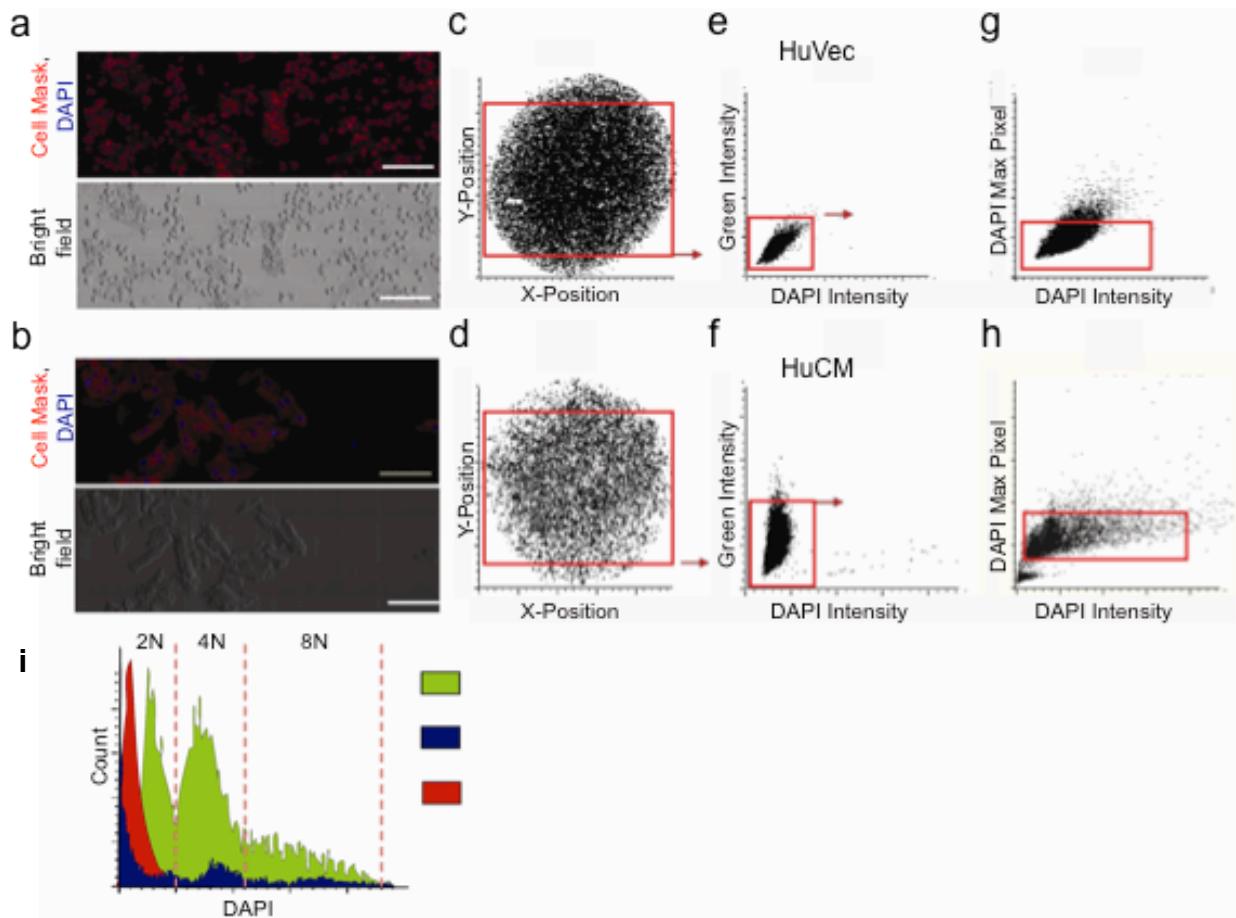
### Supplemental Figure and Legend S3, continued



### Supplemental Figure S3, continued. Validation of the immunofluorescent identification of cardiomyocytes for the optical dissector method.

Sections from human neonatal (**e**) and adult (**f**) hearts were stained with haematoxylin-eosin (H&E). Mean number of cardiomyocytes was determined per counting frame (131 x 131  $\mu\text{m}$ ) and compared to the quantification from the optical dissector method. Scale bar 25  $\mu\text{m}$ . (**g**) Bland Altman analysis demonstrates slight overestimation of cardiomyocyte counts using the haematoxylin-eosin staining versus the optical dissector with antibody against troponin I. (**h**) Bland Altman analysis shows a good agreement between troponin I and caveolin 3 in the quantification of cardiomyocytes with the optical dissector method.

## Supplemental Figure and Legend S4

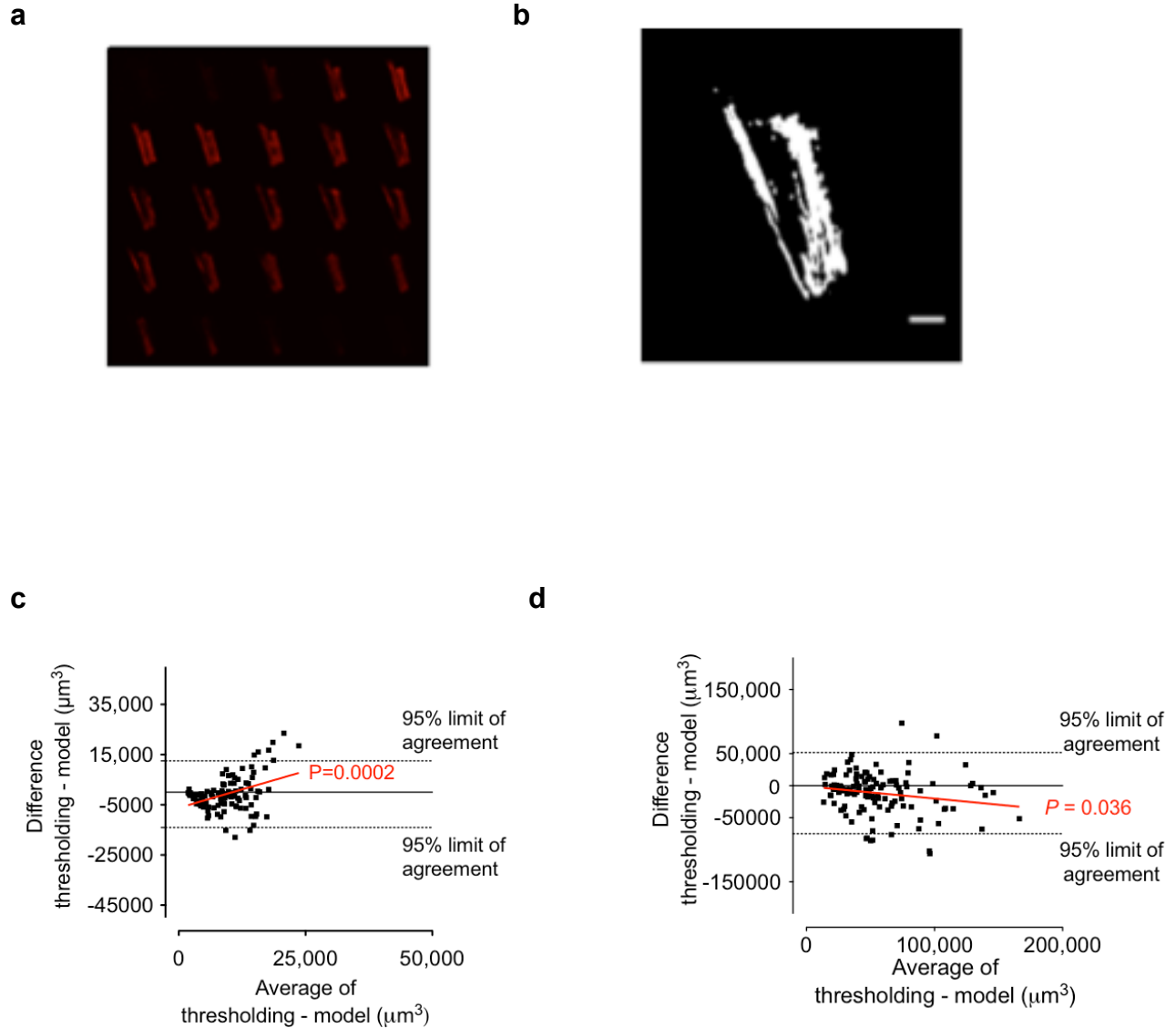


### Supplemental Figure S4. Method of ploidy quantification in isolated human cardiomyocytes using laser-scanning cytometry (LSC).

(a-e) Calibration of the method. Human umbilical cord endothelial cells (huVec), being uniformly mononucleated with diploid nuclei (2N), were used as control to determine DNA content by LSC. Isolated huVec (a,c,e,g) and cardiomyocytes (HuCM, b,d,f,h) were stained with Cellmask<sup>TM</sup> membrane dye and DAPI and spread on slides. (a, b) Representative LSC photomicrographs of immunofluorescence (top panel) and bright bright field (bottom panel). Scale bars 100  $\mu\text{m}$ . huVec (c) and cardiomyocyte (d) preparations were gated through X and Y positions and autofluorescent artefacts were excluded (e,f). Individual nuclear events were defined by threshold contouring of DAPI stained nuclei. The numbers of nuclei in each cell are defined by nuclear events within the integration contour of cellular events. The integration contour is set as 7 pixels from the threshold contour of cellular events (pixel size is 1 $\mu\text{m}$  x 0.491 $\mu\text{m}$ )(g, h). DNA content histogram (i) established by DAPI integrated fluorescence signal in cycling huVec cells (blue plot) and human cardiomyocytes (green plot). HuVec cells were synchronized in G0/G1 of the cell cycle with a double thymidine block to establish diploid DNA content threshold settings (red plot).



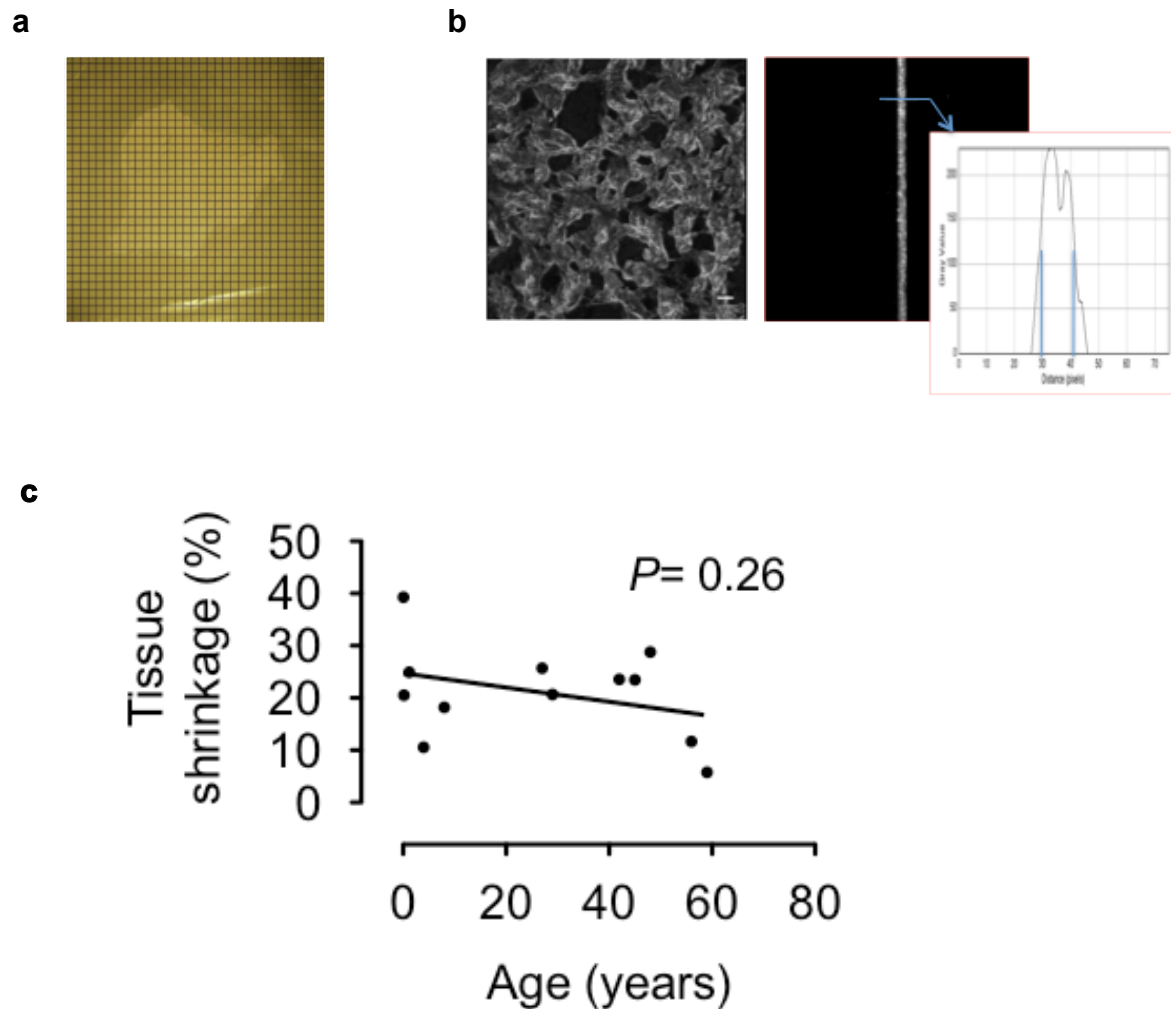
## Supplemental Figure and Legend S5



### Supplemental Figure S5. Method for quantification of mean cellular volume.

For volume determination, cardiomyocytes were isolated, stained with CellMask Orange and imaged with confocal microscopy. **(a)** Photomicrographs of all optical sections of one representative cardiomyocyte. **(b)** A single optical section used for digital color thresholding. **(c)** Comparison of agreement between design-and model-based method using Bland-Altman analysis in three neonatal hearts ( $P = 0.0002$ ). **(d)** Comparison of agreement between both methods in three adult hearts ( $P = 0.036$ ).

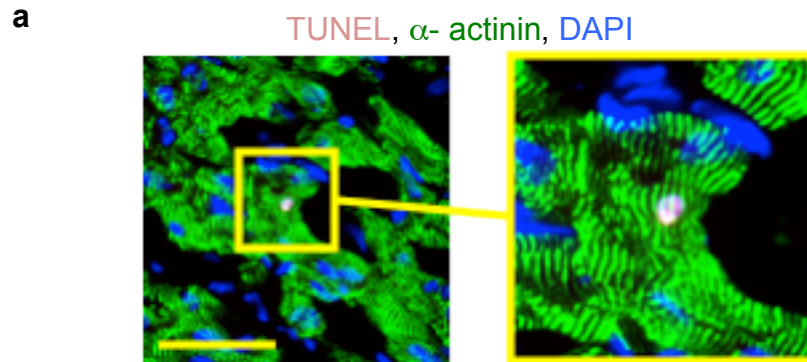
## Supplemental Figure and Legend S6



### Supplemental Figure S6. Quantification of tissue shrinkage.

(a) A representative phase contrast image of an unfixed and unstained myocardial section from HS 5.114, overlaid with a grid with known dimensions for determination of the area shrinkage via grid-point method (xy-dimensions). (b) DIC images of Z-stacks of myocardial tissue sections with orthogonal view and grey value profile for determination of FWHM (full width at half maximum) intensity. (c) Volume shrinkage (%); linear regression analysis ( $P = 0.26$ ) showed that the slope was not significantly different than 0. We calculated a mean value for tissue shrinkage of  $21 \% \pm 5.8\%$  ( $n = 12$  hearts).

## Supplemental Figure and Legend S7

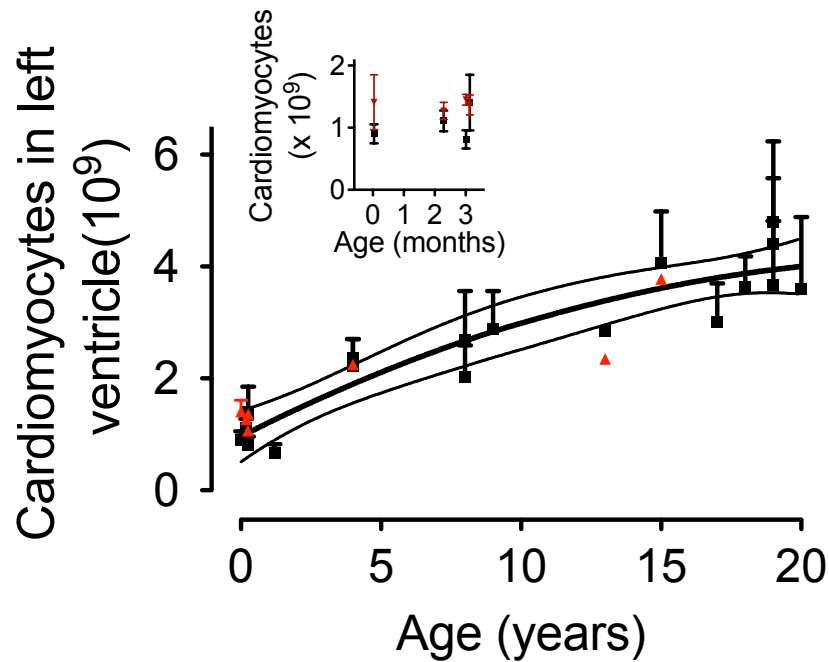


**b**

| Sample ID                                | HS21-63 | HS16-67 | HS15-67 | HS4-62 | HS14-18 |
|--|---------|---------|---------|--------|---------|
| Age (years)                              | 1.2     | 4       | 9       | 14     | 19      |
| Total Area Quantified (mm <sup>2</sup> ) | 73.15   | 69.14   | 135.12  | 120.05 | 86.65   |
| TUNEL pos events                         | 0       | 0       | 0       | 0      | 1       |

### Supplemental Figure S7. Apoptosis is not a mechanism related to physiologic heart growth

To determine whether cardiomyocyte apoptosis is a mechanism associated with myocardial growth, two slides from 5 hearts were examined for the presence of TUNEL-positive cardiomyocytes. **(a)** Representative photomicrograph from a 19-year-old individual. **(b)** Results of quantification show that TUNEL-positive cardiomyocytes are extremely rare.

**Supplemental Figure and Legend S8**

**Supplemental Figure S8. Quantifications of cardiomyocyte number per LV using calculated and actual heart weights yield similar results.**

Black dots indicate total number of cardiomyocytes per LV based on calculated heart weights from the donor's BSA. Red triangles indicate calculations based on the actual weights, which were available for 7 of the hearts. Blow-up graph of results in the first 3.5 months of life are shown.

**Supplemental Table S1. List of all hearts used in this study.**

| #   | Blinded ID | ID Number | Gender | Age     | Histopathological comment  | Cause of death                              |
|-----|------------|-----------|--------|---------|--|---|
| 1.  | HS60       | M3873M    | F      | 1 day   | Focal haemorrhage of the atrioventricular valve. No other abnormalities                                    | Stillbirth                                  |
| 2.  | HS5        | 4.087     | F      | 14 days | Normal myocardium  | Brain tumor, 11 days on life support        |
| 3.  | HS61       | 1490      | F      | 70 days | Unremarkable   | Sudden unexpected death in infancy          |
| 4.  | HS62       | 1738      | F      | 92 days | Normal myocardium  | Bronchopneumonia                            |
| 5.  | HS63       | 1055      | M      | 96 days | Unremarkable   | Bronchopneumonia                            |
| 6.  | HS21       | 5.114     | F      | 1.2 y   | Dense subendocardial fibrosis, slightly increased interstitial fibrosis                                    | Drowning (hypoxic brain injury)             |
| 7.  | HS4        | 4.043     | M      | 3 y     | Normal myocardium, no fibrosis or inflammation   | Head trauma                                 |
| 8.  | HS16       | 4.152     | M      | 4 y     | Normal myocardium  | Motor vehicle accident-brain injury         |
| 9.  | HS71       | 1185      | M      | 4y      | Unremarkable   | Drowning                                    |
| 10. | HS28       | 5.144     | F      | 4.5 y   | No perivascular and/ or interstitial fibrosis, no inflammation   | Hypoxic brain injury                        |
| 11. | HS2        | 2.090     | M      | 8 y     | Normal myocardium  | Not recorded                                |
| 12. | HS31       | 3.109     | M      | 8 y     | Normal myocardium  | Intracerebral hemorrhage                    |
| 13. | HS15       | 5.110     | M      | 9 y     | Normal myocardium, only focal fibrosis within normal limits, no necrosis, no inflammation                  | Asphyxia                                    |
| 14. | HS72       | 5173      | F      | 10y     | No pathological change   | Asthma                                      |
| 15. | HS73       | 1670      | F      | 13y     | Unremarkable   | Asphyxia by hanging                         |
| 16. | HS74       | 4638      | M      | 15y     | Unremarkable   | Motor vehicle accident                      |
| 17. | HS50       | 6.072     | M      | 16 y    | Markedly increased interstitial fibrosis   | Hanged                                      |
| 18. | HS9        | 2.158     | M      | 17 y    | Normal myocardium  | Head injury                                 |
| 19. | HS40       | 6.016     | M      | 18 y    | Slightly increased perivascular fibrosis, still within normal limits. No signs of other myocardial disease | Hypoxic brain injury-acute alcohol toxicity |
| 20. | HS20       | 3.116     | M      | 19 y    | Normal myocardium  | Motor vehicle accident                      |
| 21. | HS27       | 3.168     | F      | 19 y    | Normal myocardium  | Motor vehicle accident                      |
| 22. | HS14       | 4.015     | M      | 19 y    | Plenty of regions with replacement fibrosis-abnormal   | Hanging                                     |

| #   | Blinded ID | ID Number | Gender | Age  | Histopathological comment   | Cause of death  |
|-----|------------|-----------|--------|------|---|---|
| 23. | HS23       | 1.103     | F      | 20 y | Normal myocardium   | Subarachnoid hemorrhage   |
| 24. | HS6        | 3.160     | M      | 21 y |   | Motor vehicle accident  |
| 25. | HS1        | 5.138     | M      | 23   | Normal myocardium   | Self-strangulation  |
| 26. | HS26       | 5.015     | M      | 24   | Normal myocardium   | Not recorded  |
| 27. | HS19       | 5.048     | F      | 25   | Normal myocardium   | SAB, not transplanted due to Herpes simplex serology                        |
| 28. | HS29       | 3.135     | M      | 26   | Normal myocardium   | Subarachnoidal haemorrhage  |
| 29. | HS7        | 2.116     | F      | 27   | Normal myocardium   | Seizure   |
| 30. | HS13       | 5.054     | M      | 27   | Normal myocardium   | Seizure   |
| 31. | HS32       | 5.086     | M      | 29   | Normal myocardium   | Hypoxic brain injury  |
| 32. | HS3        | 5.003     | M      | 37   | Normal myocardium   | Intracerebral haemorrhage   |
| 33. | HS34       | 3.069     | F      | 40   | Slightly increased focal, but no interstitial fibrosis. No necrosis. No inflammation. | Middle cerebral artery infarction   |
| 34. | HS12       | 5.041     | F      | 42   | Normal myocardium   | Subarachnoidal haemorrhage  |
| 35. | HS18       | 1.095     | F      | 45   | Normal myocardium   | Not recorded  |
| 36. | HS36       | 5.089     | F      | 48   | Normal myocardium   | Subarachnoidal haemorrhage, no transplanted due to AB group incompatibility |
| 37. | HS24       | 6.004     | M      | 48   | Markedly increased fibrosis   | Hypoxic brain injury  |
| 38. | HS11       | 3.141     | M      | 52   | Normal myocardium   | Intracerebral haemorrhage   |
| 39. | HS30       | 4.155     | M      | 56   | Normal myocardium   | Hanging   |
| 40. | HS17       | 4.104     | F      | 59   | Normal  | Not recorded  |

**Legend to Supplemental Table S1.** Myocardial tissue was provided by the NICHD Brain and Tissue Bank for Developmental Disorders at the University of Maryland and the University of Sydney. The samples were subjected to pathological evaluation and confirmed free of disease. Samples with increased fibrotic contents were taken out of the study (red).

## Supplemental Table S2. Image acquisition hardware and settings.

|            | Hardware   | Software and settings                        |
|------------|--|--|
| Fig 1a-c   | Olympus IX-81 epifluorescence microscope <sup>3</sup> with UPLFL ×10, and LUCPLFL ×40, NA 0.6 lenses and equipped with Hamamatsu EM CCD C9100                                  | 20–400 msec exposure, Slidebook <sup>2</sup> |
| Fig. 2 a,b | Olympus IX-81 epifluorescence microscope <sup>3</sup> with UPLFL ×10, and LUCPLFL ×40, NA 0.6 (immunofluorescence micrographs) lenses and equipped with Hamamatsu EM CCD C9100 | 20–400 msec exposure, Slidebook <sup>2</sup> |
| Fig. 3a    | Olympus Fluoview 1000 epifluorescence microscope, 60x water objective, NA 1.2  | 100-600 msec exposure, Olympus software      |
| Fig. 4c    | Olympus IX-81 epifluorescence microscope <sup>3</sup> with UPLFL ×10, and LUCPLFL ×40, NA 0.6 (immunofluorescence micrographs) lenses and equipped with Hamamatsu EM CCD C9100 | 20–400 msec exposure, Slidebook <sup>2</sup> |

**Legend to Supplemental Table S2.** Key to manufacturers: <sup>1</sup> Hewlett-Packard and Acuson; <sup>2</sup> Intelligent Imaging Innovations, Inc., Denver, CO; <sup>3</sup> CompuCyte, Westwood, MA

**Supplemental Table S3. Quantification of numeric data.**

| <b>Figure</b> | <b>Assay</b>   | <b>Number of cardiomyocytes and/or hearts analyzed</b>  |
|---------------|--|---|
| Fig.1d        | Fibrosis analysis  | 24 hearts analyzed, 20 sections per heart, 15 random images per section                             |
| Fig. 1e-f     | Spot-to-spot variability of number of nuclei in different spots of the same LV | 15 random systematic sections from 3 different, non adjacent parts of the LV                        |
| Fig. 2c       | Mitotic cardiomyocytes (LSC)   | 651,160 cardiomyocytes  |
| Fig. 3b       | MKLP-1 positive events   | 15 images per sections analyzed, 20 sections per heart  |
| Fig 4a        | LSC validation of mononucleation assessment                                    | 1,500 cardiomyocytes manually counted from 5 different hearts                                       |
| Fig. 4b       | Mononucleated cardiomyocytes   | 220,989 cardiomyocytes  |
| Fig. 4d       | Cardiomyocyte ploidy validation by FISH  | 500 cardiomyocytes from 5 different hearts for each chromosome-specific probe (chromosomes X and 8) |
| Fig. 4e-f     | Polyploid cardiomyocytes   | Appr. 15 000 cardiomyocytes per sample counted  |
| Fig. 5a       | Cardiomyocyte nuclear density by optical dissector                             | 3 random images of 5 sections (15 sample volumes per heart)   |
| Fig. 5b       | Cardiomyocyte nuclei   | 3 random images of 5 sections (15 sample volumes per heart)   |
| Fig. 5c       | Number of cardiomyocytes in LV   | 3 random images of 5 sections (15 sample volumes per heart)   |
| Fig. 5d       | Mean cardiomyocyte volume  | 1,928 cardiomyocytes  |

**Supplemental Table S4. Antibody manufacturers and dilutions.**

| <b>Antibody/dye</b>                               | <b>Manufacturer</b>                     | <b>Dilution/concentration</b> |
|---|---|-------------------------------|
| Phosphorylated histone H3 at Ser10 (H3P)          | Millipore                               | 1:500                         |
| MKLP-1  | Abcam                                   | 1:100                         |
| Sarcomeric $\alpha$ -actinin ( $\alpha$ -actinin) | Sigma                                   | 1:500                         |
| Tropomyosin CH1 (TM)                              | Developmental Studies<br>Hybridoma Bank | 1:100                         |
| Pan-cadherin (Cat #C3678)                         | Sigma                                   | 1:500                         |
| Caveolin 3 (Cat #610421)                          | BD Transduction Labs                    | 1:100                         |
| Alexa- conjugated secondary antibodies            | Invitrogen                              | 1:200 to 1:500                |
| DAPI  | Invitrogen                              | 50 nM                         |
| Cell mask orange                                  | Invitrogen                              | 5 $\mu$ g/mL                  |

**Supplemental Table S5.** Comparison of quantitative data of recent studies of cardiomyocyte generation and renewal in humans without evidence for heart disease.

| Age         | Number of hearts/Results | Bergmann et al., 2009                                |          |         | Kajstura et al., 2012, non-failing hearts            |             |         | Mollova, Bersell et al., non-failing hearts |                 |  |
|-------------|--------------------------|--|----------|---------|--|-------------|---------|---|-----------------|--|
|             |                          | Predicted CM generation (% per year) <sup>14C*</sup> | Ki67 (%) | H3P (%) | Predicted CM generation (% per year) <sup>14C*</sup> | Isolated CM | H3P (%) | Isolated CM <sup>†</sup>                    | Cytokinesis (%) | Predicted CM generation (% per year) <sup>H3P§</sup> |
| 0-1 years   | Number of hearts studied | 0  | 0        | 0       | 0  | 0           | 6       | 6   | 6               | 6  |
|             | Results                  | -  | -        | -       | -  | -           | 0.04%   | 0.015%                                      | 0.015%          | 100%   |
| 1-10 years  | Number of hearts studied | 2 (1, 6 years)                                       | 3        | 3       | 3  | 3           | 4       | 4   | 4               | 4  |
|             | Results                  | NA   | 0.15%    | 0.01%   | 21%  | 0.01%       | 0.02%   | 0.01%                                       | 0.01%           | 4.5%   |
| 10-20 years | Number of hearts studied | 1 (19 years old)                                     | 2        | 2       | 2  | 2           | 5       | 5   | 5               | 5  |
|             | Results                  | 1.9%   | 0.05%    | 0.004%  | 9%   | 0.004%      | 0.01%   | 0.005%                                      | 0.005%          | 1.6%   |
| 21-40 years | Number of hearts studied | 5  | 2        | 2       | 2  | 2           | 12      | 6   | 6               | 12   |
|             | Results                  | 1%   | 0.04%    | 0.003%  | 6%   | 0.003%      | 0.01%   | Not detectable                              | Not detectable  | 0.7%   |
| >40 years   | Number of hearts studied | 6  | 12       | 12      | 12   | 12          | 3       | 3   | 3               | 3  |
|             | Results                  | 0.5%   | 0.07%    | 0.006%  | 5.6%   | 0.006%      | 0.001%  | Not detectable                              | Not detectable  | 0.04%  |

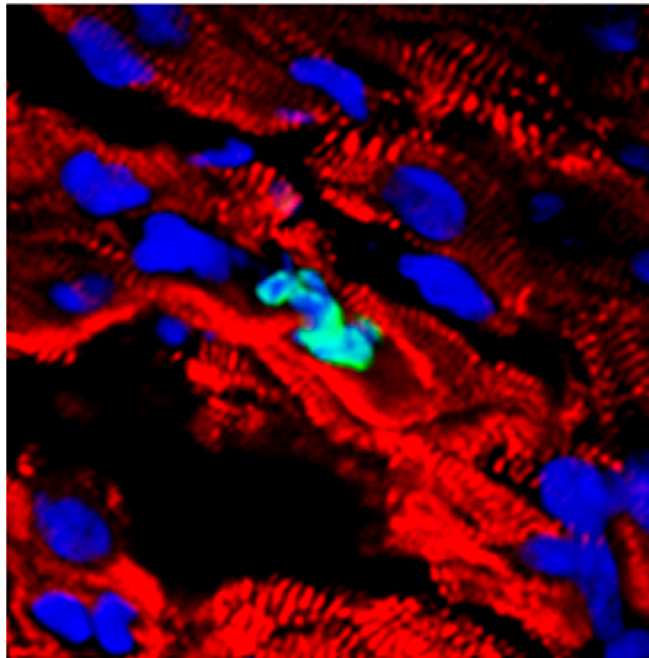
**Legend:** \* Cardiomyocyte generation was calculated by birth-dating of cardiomyocytes based on the mean <sup>14</sup>C-concentration in nuclear DNA. <sup>†</sup> H3P data were obtained with laser scanning cytometry (LSC). <sup>§</sup> Cardiomyocyte generation was calculated from the prevalence of H3P cardiomyocytes, corrected for multinucleation and polyploidization. Since above the age of 20 years, we did not detect cytokinesis, this suggests either of two possibilities: none of the H3P events resulted in cardiomyocyte division or our cytokinesis assay, although sensitive enough to detect 0.005% cardiomyocyte cytokinesis, is not sensitive enough to detect the low frequency of cardiomyocyte cytokinesis in adult hearts.

## REFERENCES

1. Howard CV, Reed M (2005) *Unbiased Stereology: Three-Dimensional Measurement In Microscopy*. Oxford: BIOS Scientific Publishers.
2. Grierson AM, Mitchell P, Adams CL, Mowat AM, Brewer JM, et al. (2005) Direct quantitation of T cell signaling by laser scanning cytometry. *J Immunol Methods* 301: 140-153.
3. Haycock GB, Schwartz GJ, Wisotsky DH (1978) Geometric method for measuring body surface area: a height-weight formula validated in infants, children, and adults. *J Pediatr* 93: 62-66.
4. Muhlfield C, Nyengaard JR, Mayhew TM (2010) A review of state-of-the-art stereology for better quantitative 3D morphology in cardiac research. *Cardiovasc Pathol* 19: 65-82.
5. Sluysmans T, Colan SD (2005) Theoretical and empirical derivation of cardiovascular allometric relationships in children. *J Appl Physiol* 99: 445-457.
6. Foster BJ, Mackie AS, Mitsnefes M, Ali H, Mamber S, et al. (2008) A novel method of expressing left ventricular mass relative to body size in children. *Circulation* 117: 2769-2775.

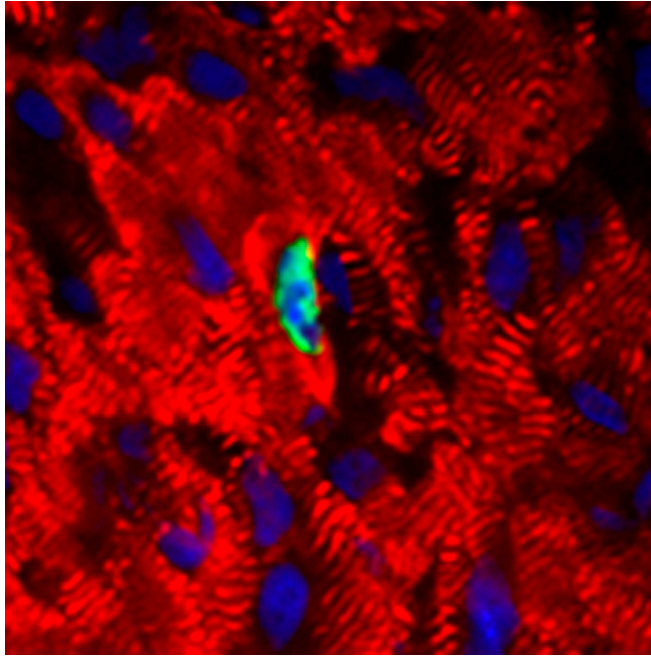
# Supporting Information

Mollova et al. 10.1073/pnas.1214608110



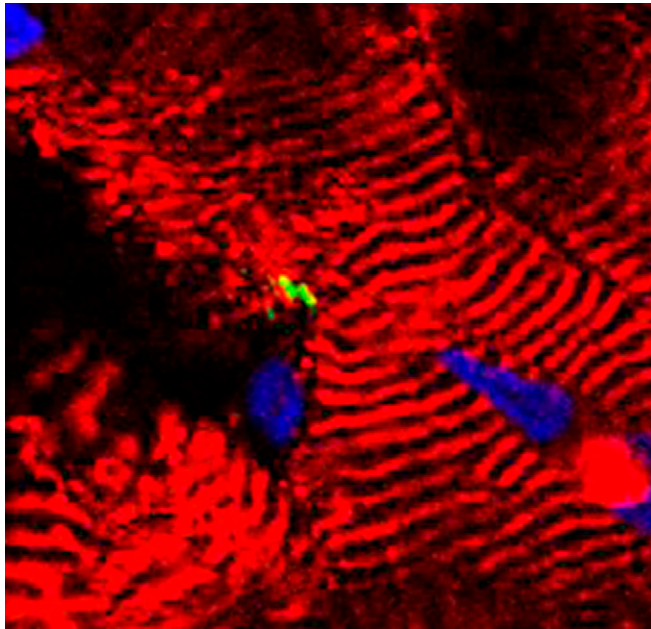
**Movie S1.** This movie shows a rotational 3D reconstruction of an H3P-positive cardiomyocyte nucleus. One level from this stack is shown in the second row of Fig. 2B.

[Movie S1](#)



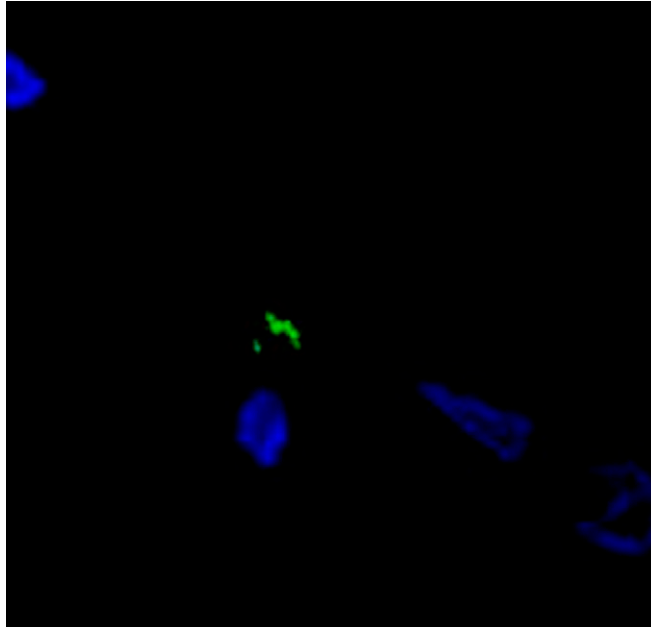
**Movie S2.** This movie shows a rotational 3D reconstruction of an H3P-positive cardiomyocyte nucleus. One level from this stack is shown in the third row of Fig. 2B.

[Movie S2](#)



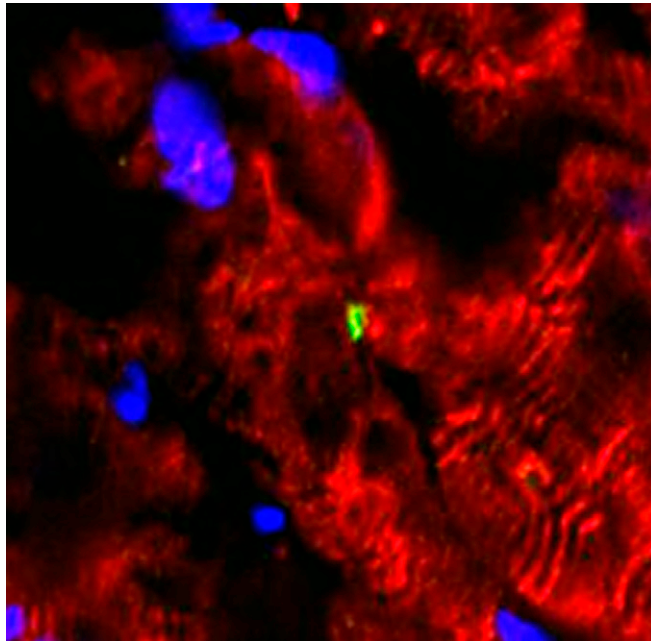
**Movie S3.** This movie is a confocal stack from which one level is shown in the left panel of Fig. 3A (from a 3-wk-old subject). The movie shows an MKLP-1-positive contractile ring.

[Movie S3](#)



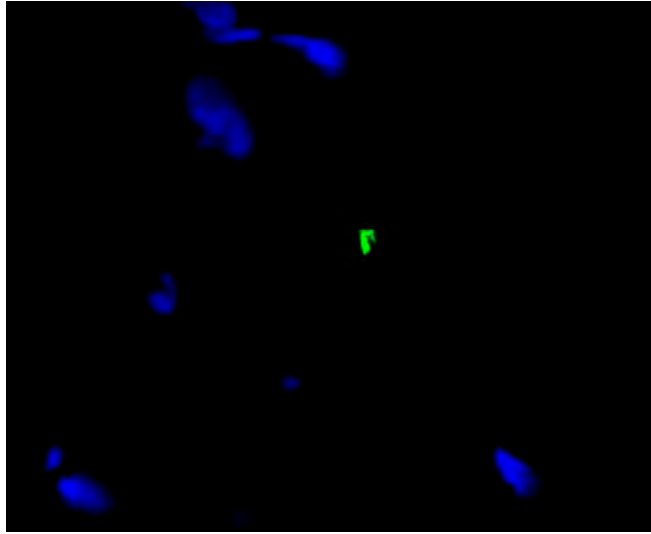
**Movie S4.** This movie is the rotational 3D reconstruction of the confocal stack shown in the left panel of Fig. 3A and [Movie S3](#). This movie shows the contractile ring in relation to cardiomyocyte nuclei. The sarcomere staining was excluded.

[Movie S4](#)



**Movie S5.** This movie is a confocal stack from which one level is shown in the right panel of Fig. 3A (from a 1.2-y-old subject). The movie shows an MKLP-1-positive contractile ring.

[Movie S5](#)



**Movie S6.** This movie is the rotational 3D reconstruction of the confocal stack shown in the right panel of Fig. 3A and [Movie S5](#). This movie shows the contractile ring in relation to cardiomyocyte nuclei. The sarcomere staining was excluded.

[Movie S6](#)

## Other Supporting Information Files

[SI Appendix \(PDF\)](#)